nature neuroscience

Neural reactivations during sleep determine network credit assignment

Tanuj Gulati[1–3], Ling Guo[1–3], Dhakshin S Ramanathan[1,3–5], Anitha Bodepudi[1,2] & Karunesh Ganguly[1–3]

A fundamental goal of motor learning is to establish the neural patterns that produce a desired behavioral outcome. It remains unclear how and when the nervous system solves this 'credit assignment' problem. Using neuroprosthetic learning, in which we could control the causal relationship between neurons and behavior, we found that sleep-dependent processing was required for credit assignment and the establishment of task-related functional connectivity reflecting the casual neuron–behavior relationship. Notably, we observed a strong link between the microstructure of sleep reactivations and credit assignment, with downscaling of non-causal activity. Decoupling of spiking to slow oscillations using optogenetic methods eliminated rescaling. Thus, our results suggest that coordinated firing during sleep is essential for establishing sparse activation patterns that reflect the causal neuron-behavior relationship.

Hallmarks of learning a new skill include a substantial reduction of movement variability and a concomitant reduction in both the extent and variability of neural firing[1–7]. This process is associated with increasingly sparse task-related neural activation patterns[5–8]. A theoretical framework for the underlying computation is frequently labeled the 'credit assignment' problem, that is, determination of how a single neuron in a highly interconnected biological network causes a behavior[9,10]. Past work has suggested that a key goal of credit assignment is to select neural activity that truly reflects the causal neuron-behavior relationship[8,11]. However, it remains unknown how a complex and interconnected biological neural network can solve this computation.

We hypothesized that sleep-dependent reactivations might be important for network credit assignment. A large body of work indicates that sleep is important in memory consolidation[12–14]. More specifically, reactivation of neural activity during sleep has been implicated in memory consolidation[12,14–17]. However, there has been a great deal of debate regarding the specific computational role of such reactivations[12–14]. Two commonly cited possibilities are that sleep-dependent reactivations lead to a general strengthening of functional connectivity or a process of renormalization with both strengthening and weakening of functional connectivity[12,14,18]. In the case of renormalization, a theoretical prediction is that, after a period of sleep, there may be rescaling of task-related activity (for example, neural activations not causally linked to performance are selectively downscaled)[18]. Notably, such a process of rescaling of task activations could be used for network credit assignment.

Here we used a neuroprosthetic-learning task, in which the 'decoder' and the causality of the neuron-behavior relationship are set by the experimenter[8,11,19–24], to evaluate whether NREM sleep has a role in credit assignment. Unlike natural motor behaviors, neuroprosthetic control offers a unique method for studying plasticity; a small set of neurons is chosen to causally control actuator movements (that is, 'direct' neurons)[8,19]. In contrast, 'indirect' neurons show task-related activity even though they do not cause actuator movements[8,11,25]. Notably, although past work has shown that learning proficient control through putative error-correction processes leads to increased activity of direct neurons and diminished activity of indirect neurons[8,11,20,25,26], it remains unclear how and when this fundamental credit-assignment process is solved. We found that neural spiking triggered by slow oscillations during sleep is essential for credit assignment.

RESULTS

Rescaling of task activity

In five rats implanted with microwire arrays in primary motor cortex (M1), we monitored sets of direct (TR_D) and indirect (TR_I) neurons during the initial learning (hereafter referred to as BMI_1), during a period of sleep and during subsequent task performance following awakening (hereafter referred to as BMI_2). A linear decoder with randomized weights converted the firing rates of two randomly chosen TR_D neurons into the angular velocity of the actuator. The decoder weights were held constant during the session to exclusively rely on neural learning. Notably, there has been a study demonstrating that decoder adaptation can still induce long-term plasticity[27]. However, this study was done in non-human primate models performing more complex tasks. In our experiments, rats were trained to control the angular velocity of a feeding tube via modulation of neural activity. At the start of each trial, the angular position of the tube was set to 0° (P_1; **Fig. 1a**,**b**). If the angular position of the tube was held for >300 ms at position P_2 (90°), a defined amount of water was delivered (that is, a successful trial); a trial was stopped if this was not achieved within

[1]Neurology and Rehabilitation Service, San Francisco Veterans Affairs Medical Center, San Francisco, California, USA. [2]Department of Neurology, University of California-San Francisco, San Francisco, California, USA. [3]Center for Neural Engineering and Prostheses, University of California-Berkeley and University of California-San Francisco, California, USA. [4]Department of Psychiatry, San Francisco Veterans Affairs Medical Center, San Francisco, California, USA. [5]Department of Psychiatry, University of California-San Francisco, San Francisco, California, USA. Correspondence should be addressed to K.G. (karunesh.ganguly@ucsf.edu).

Received 22 June 2016; accepted 23 May 2017; published online 10 July 2017; doi:10.1038/nn.4601

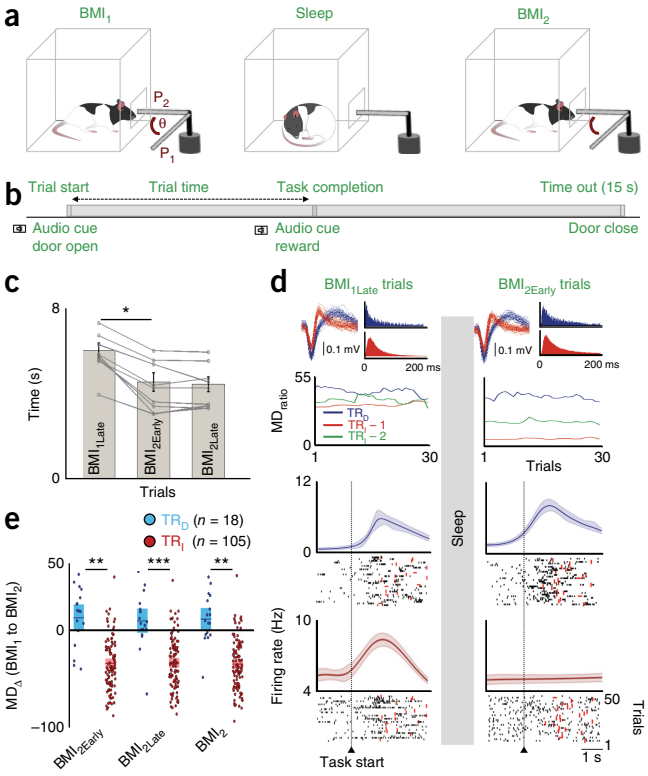

Figure 1 Rescaling of task activations after sleep. (**a**) The practice sessions were separated by a block of sleep. Rats learned direct neural control of a feeding tube (θ = angular position). Successful trials required movement from P_1 to P_2 within 15 s. (**b**) A typical trial structure is depicted. (**c**) Comparison of trial times. A significant reduction in completion time was found between BMI_{1Late} to BMI_{2Early} ($n = 10$ sessions; paired t test, $t_9 = 7.62$, $^*P < 10^{-4}$). Bar plot shows mean ± sem. (**d**) At the top are the waveforms and inter-spike interval histograms of the neurons analyzed below (color coded). Plot below shows the trend in the modulation depth ratio (MD_{ratio}) during BMI performance for three neurons before and after sleep. Another neuron whose waveform is not shown is depicted in green. Shown below are the PETHs from BMI_{1Late} and BMI_{2Early} trials for the TR_D and TR_I neurons, respectively (in same color convention). Thick line represents mean; shaded area is the jackknife error. Below the PETHs are representative spike rasters from multiple trials. Red dot indicates task completion time for each trial. (**e**) Average modulation depth change (MD_Δ) between BMI_1 and BMI_2 (mean in solid line ± s.e.m. in box; unpaired t tests; BMI_1 and BMI_{2Early}, $t_{121} = 6.79$, $^{**}P < 10^{-9}$; BMI_1 and BMI_{2Late}, $t_{121} = 6.31$, $^{***}P < 10^{-8}$; BMI_1 and BMI_2, $t_{121} = 6.96$, $^{**}P < 10^{-9}$).

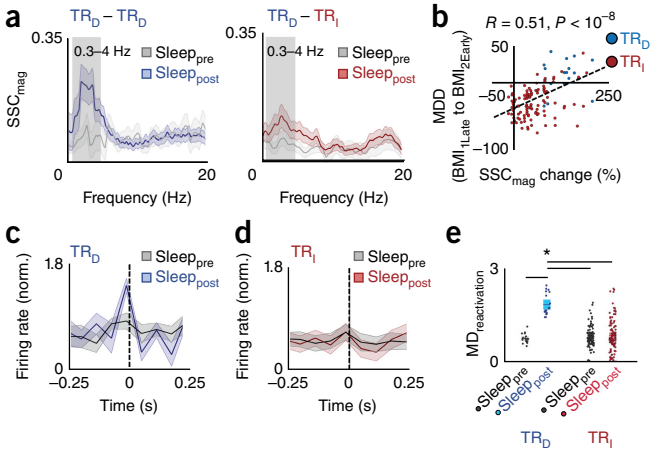

Figure 2 Changes in functional connectivity of direct neuronal pairs and reactivation microstructure. (**a**) Example plot of SSC as a function of frequency during sleep before ($Sleep_{pre}$) and after ($Sleep_{post}$ for $TR_D - TR_D$; red for $TR_D - TR_I$ pairs) skill acquisition. The lighter band is the jackknife error. The box highlights the 0.3–4-Hz band. (**b**) Relationship between SSC change before and after learning, and change in task-related modulation after sleep, $MD_\Delta(BMI_{1Late}$ to $BMI_{2Early})$, Spearman correlation, $r(123) = 0.51$, $P < 10^{-8}$. (**c**) Average modulation depth during reactivations ($MD_{reactivation}$, that is, ratio of peak to tails) of TR_D neurons from $Sleep_{pre}$ to $Sleep_{post}$. (**d**) $MD_{reactivation}$ of TR_I neurons from $Sleep_{pre}$ to $Sleep_{post}$. (**e**) Average modulation depth during $Sleep_{pre}$ to $Sleep_{post}$ reactivations for TR_D and TR_I neurons (mean in solid line ± s.e.m. in box, one-way ANOVA, $F_{3,242} = 34.28$, $P < 10^{-17}$; significant *post hoc* t tests, $^*P < 0.05$).

15 s. Over a typical 2-h session, animals were able to learn the task. Consistent with previous results[23], after a period of NREM sleep, task performance improved at the start of BMI_2 (also referred to as BMI_{2Early}; **Fig. 1c**; $P < 0.05$ for each of the ten individual comparisons of BMI_{1Late} and BMI_{2Early}; overall paired t test, $t_9 = 7.62$, $P < 10^{-4}$).

We next compared the activity of TR_D and TR_I neurons during task performance immediately before and after sleep (that is, intervening sleep or $Sleep_{post}$, duration: 36.94 ± 1.06 min, mean ± s.e.m., $n = 10$ sessions; paired t test of $Sleep_{pre}$ and $Sleep_{post}$ durations: $t_9 = 0.056$, $P = 0.95$). We specifically measured the change in the peak-firing rate during task performance relative to the baseline rate before the 'GO' cue (that is, 'modulation depth' or MD). The majority of TR_D cells increased their modulations (~67%), whereas a majority of TR_I cells reduced their modulation (~90%). Notably, although TR_D neurons experienced a slight, but significant, increase in modulation depth (7.39 ± 5.89%, Wilcoxon signed-rank test, $Z = -1.81$, $P = 0.03$), there was a substantial net decrease in the MD of TR_I neurons (−31.76 ± 2.18%, paired t test, $t_{104} = 14.58$, $P < 10^{-26}$) (**Fig. 1d,e**). In addition, we found that the time spent in sleep predicted the extent of TR_I downscaling (Spearman correlation, $r = -0.71$, $P < 0.05$).

Changes in functional coupling during sleep

We next compared the changes in functional connectivity in the recorded M1 neural ensembles during NREM sleep epochs before and after training. We specifically calculated the magnitude of spike-spike coherence (SSC) for $TR_D - TR_D$ and $TR_D - TR_I$ pairs both during the sleep that followed training ($Sleep_{post}$) and the sleep that preceded training ($Sleep_{pre}$). The SSC is a pairwise measure of how phase-locked two neurons are across of frequencies[28]. For $TR_D - TR_I$, pairs, the TR_D neuron with stronger task-related modulation was chosen for SSC calculation relative to the other TR_I neurons. We observed that the $Sleep_{post}$ SSC curves for $TR_D - TR_D$ unit pairs showed a significant increase in the 0.3–4-Hz band (**Fig. 2a**); this frequency band reflects slow-oscillatory activity during NREM sleep[13,14]. At the population level, these increases were greater for $TR_D - TR_D$ pairs than for $TR_D - TR_I$ pairs (129.78 ± 10.29% increase for $TR_D - TR_D$ pairs and 56.30 ± 4.73% increase for $TR_D - TR_I$ pairs; unpaired t test, $t_{121} = 6.95$, $P < 10^{-7}$). We observed no significant differences near the spindle band (8–20 Hz) or ripple (100–300 Hz) frequency bands (data not shown). This indicates that the decoder-coupled direct units (that is, $TR_D - TR_D$) were significantly more likely to fire synchronously during slow oscillations in relation to their coupling with indirect units (that is, $TR_D - TR_I$) during $Sleep_{post}$. We also found that the firing rate of the neurons did not significantly change between the two epochs (mean firing rate for the two epochs: 6.54 ± 0.66 to 6.62 ± 0.64 Hz, paired t tests, TR_D neurons: $t_{17} = -1.65$, $P = 0.11$; TR_I neurons: $t_{104} = 0.049$, $P = 0.96$). This may be consistent with a recent study regarding the firing changes in NREM[29], where firing rate changes were evident

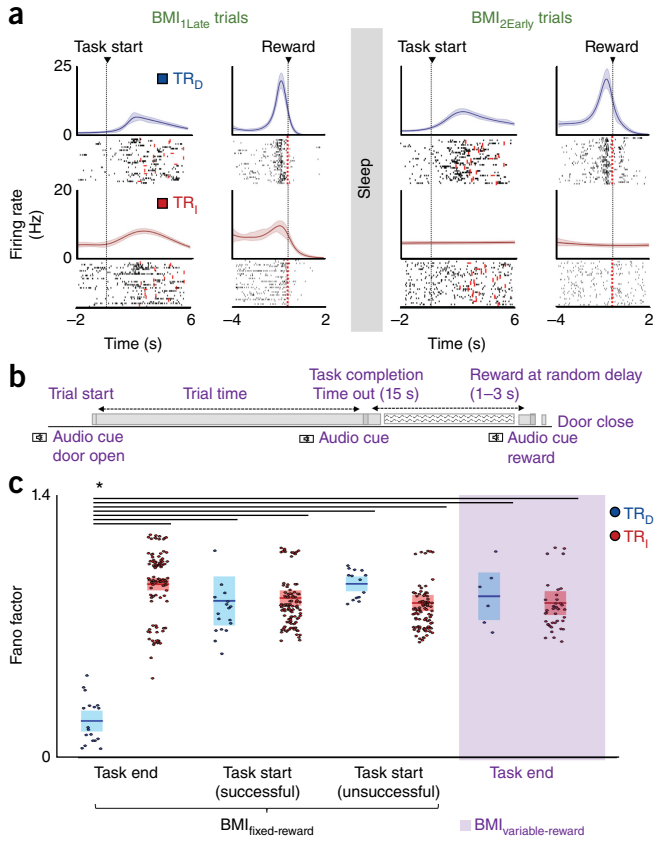

Figure 3 Consistency of reward and frames of reference. (**a**) Neural firing centered to task start and task end/reward for the same session for regular BMI training (that is, $BMI_{fixed\text{-}reward}$). The lighter band is the jackknife error. (**b**) Schematic of variable-reward BMI trials. (**c**) Average Fano factor of TR_D and TR_I neurons for the four sets of conditions, namely task start (successful and unsuccessful trials are separately parsed) and task end/reward frame in $BMI_{fixed\text{-}reward}$, and task end in $BMI_{variable\text{-}reward}$ (mean in solid line ± s.e.m. in box, task start and task end in $BMI_{fixed\text{-}reward}$ one-way ANOVA, $F_{5,350} = 41.20$, $P < 10^{-32}$; task end in $BMI_{fixed\text{-}reward}$ and $BMI_{variable\text{-}reward}$ one-way ANOVA, $F_{3,166} = 83.86$, $P < 10^{-32}$, significant *post hoc t* tests, $^*P < 0.05$).

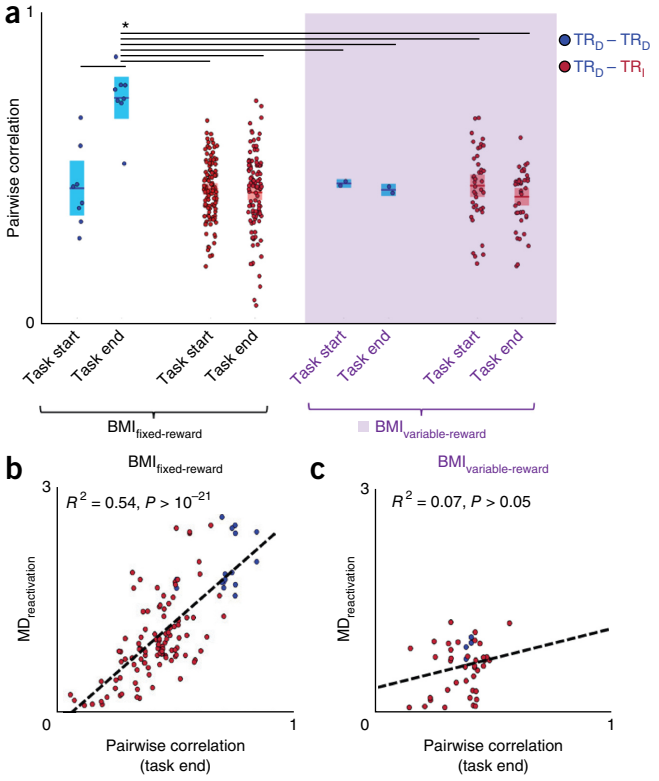

Figure 4 Pairwise correlation of neural firing during task performance and reactivations during sleep. (**a**) Pairwise correlation of neural firing for TR_D – TR_D and TR_D – TR_I pairs around task start and task end in $BMI_{fixed\text{-}reward}$ and $BMI_{variable\text{-}reward}$ procedures (mean in solid line ± s.e.m. in box; one-way ANOVA, $F_{7,304} = 8.36$, $P < 10^{-8}$; significant *post hoc t* tests, $^*P < 0.05$). (**b**) Relationship of individual neural pairwise (that is, at task end) and reactivation during sleep in $BMI_{fixed\text{-}reward}$ sessions (linear regression $R^2 = 0.54$, $P < 10^{-21}$; neural pairs are in same convention as in **Fig. 4a**). (**c**) Relationship of individual neural pairwise correlations at task end and reactivation during sleep in $BMI_{variable\text{-}reward}$ sessions (linear regression $R^2 = 0.07$, $P > 0.05$; neural pairs are in same convention as in **Fig. 4a**).

during certain phases of sleep and with monitoring of firing rates during the entire sleep period.

We next asked whether individual pairwise changes in post-learning functional connectivity could predict rescaling. As indicated above, for each neuron we calculated a single SSC value by using a single TR_D neuron as a 'reference'. Thus, we examined whether the specific changes in SSC could predict the MD changes for TR_D and TR_I units from BMI_1 to BMI_2 (**Fig. 2b**). Notably, we found that SSC changes were a strong predictor for rescaling (Pearson correlation, $r = 0.51$, $P < 0.05$), indicating that functional connectivity changes during sleep could account for the changes we observed in task activations after sleep.

We also examined whether the precisely temporal pattern of spiking (that is, microstructure) of sleep reactivations[23,30,31] could also predict rescaling. In contrast with the general functional connectivity analysis, this approach is based on the detection of temporally precise 'reactivation events' that reflect the firing patterns that emerge with learning[23,30,31]. Notably, we previously found that such reactivation events are also tightly related to slow oscillations[23]. We specifically used principal components analysis to create a template to reflect the ensemble activity that emerged with learning[23,30,31]. Subsequently, we evaluated the instantaneous reactivation strength during the two sleep epochs. We further measured the microstructure by binning the neural activity identified using reactivation analysis (that is, using coarser time bins of 50 ms) with smaller time bins of 5 ms. In principle, it is possible that the average microstructure of reactivations could resemble activity during BMI_1, resemble activity during BMI_2 or evolve over time during sleep. Detailed analysis of the identified reactivation events revealed that there was no evolution of patterns in sleep (data not shown).

We next examined whether the microstructure of reactivation events more closely resembled task-activity during BMI_1 or during BMI_2. We therefore examined the specific modulation of TR_D and TR_I neurons during the high-percentile reactivation events (Online Methods). We found that, at the population level, modulation of TR_D neurons was significantly greater around the reactivation events than for TR_I, thereby resembling the task activations evident during BMI_2. In other words, the identified reactivation events did not resemble BMI_1, where there was similar modulation of TR_D and TR_I. Modulation of TR_D neurons was also greater than in $Sleep_{pre}$, whereas they remained unchanged for the TR_I population from $Sleep_{pre}$ to $Sleep_{post}$ (one-way ANOVA, $F_{3,242} = 34.28$, $P < 10^{-17}$; **Fig. 2c–e**). Such

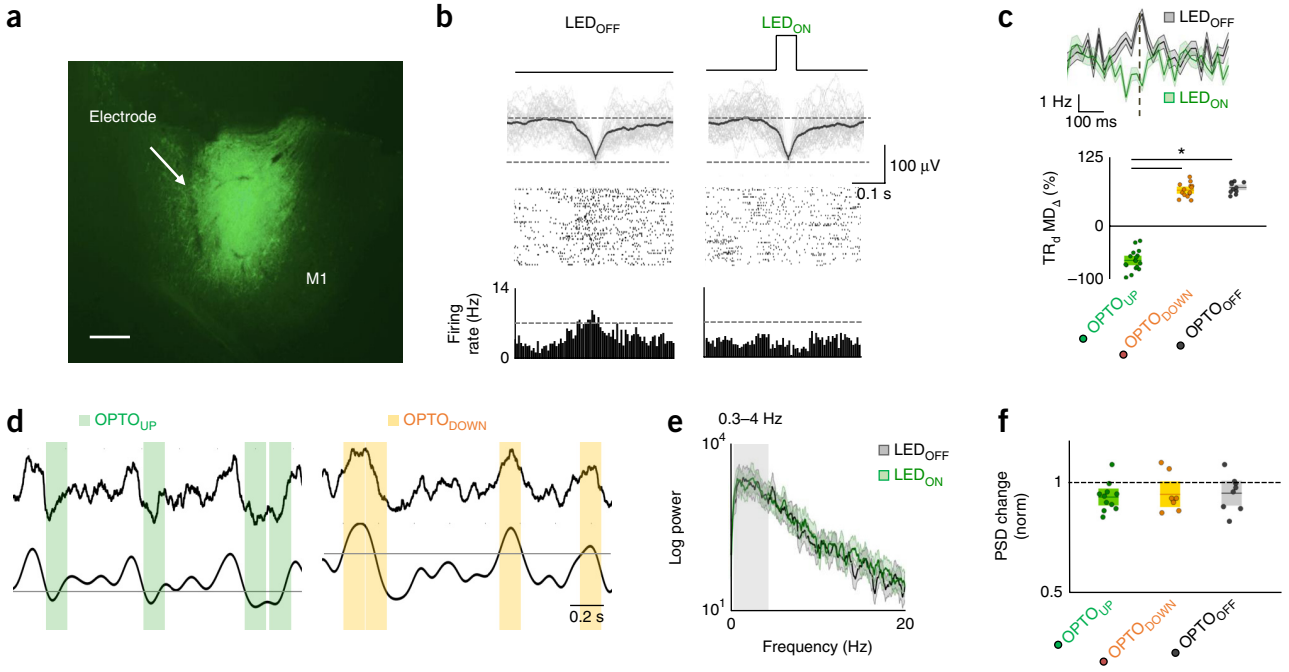

Figure 5 Optogenetic inhibition of neural activity during sleep. (**a**) Fluorescence image of a coronal brain section showing neurons expressing Jaws (green) in M1. Scale bar represents 500 µm. (**b**) UP state triggered LED inhibition of a TR_D cell in $Sleep_{post}$ as compared with the activity of same cell in $Sleep_{pre}$ without stimulation. Rasters are shown along with raw traces of the LFPs based on threshold crossing of the LFP. Dark line is the mean LFP. Bottom-most row shows histogram of firing activity. (**c**) Top, average modulation depth (MD) of a TR_D cell in a representative $OPTO_{UP}$ experiment. Shaded area is s.e.m. Bottom, average modulation depth (MD) of TR_D cells around slow-oscillations in $OPTO_{UP}$, $OPTO_{DOWN}$ and $OPTO_{OFF}$ experiments (mean in solid line ± s.e.m. in box, one-way ANOVA, $F_{2,41} = 425.75$, $P < 10^{-27}$; significant *post hoc t* tests, $^*P < 0.05$). (**d**) Examples of the raw and filtered (0.3–4 Hz) traces and the stimulation period for respective $OPTO_{UP}$ and $OPTO_{DOWN}$ experiments. (**e**) Power spectrum of LFP from $Sleep_{pre}$ and $Sleep_{post}$ in an $OPTO_{UP}$ experiments. The lighter band is the jackknife error. (**f**) Power spectral changes (in 0.3–4 Hz) for $OPTO_{UP}$, $OPTO_{DOWN}$ and $OPTO_{OFF}$ experiments (one-way ANOVA, $F_{2,27} = 0.13$, $P = 0.87$).

increased modulation was not apparent in randomly selected parts of $Sleep_{post}$ (unpaired *t* test, $t_{121} = -0.69$, $P = 0.49$; **Supplementary Fig. 1**). Taken together, these results suggest that, after learning, firing patterns generated by sleep reactivations resemble, on average, the rescaled pattern. Notably, at the level of single neurons, the depth of modulation during reactivations (**Fig. 2c–e**) predicted how a neuron changed its task-related firing rate during BMI_2 (that is, significant relationship between lack of firing during reactivations and downscaling of task activity, linear regression, $R^2 = 0.17$, $P < 10^{-5}$; **Supplementary Fig. 2**). Thus, we found that direct task-related units fired more coherently during sleep, as indicated by the elevated SSC, as well as more robustly around reactivations, and their relative modulation depth were significantly greater than for indirect units during task performance in BMI_2.

The role of reward

What determines the microstructure of reactivations? We first compared the differences between TR_D and TR_I firing during BMI_1; it was difficult to distinguish the two populations on the basis of the evolution of firing patterns locked to trial onset (**Fig. 3**). However, given that recent studies have suggested that neural activity linked to reward can be preferentially reactivated[32–34], we also compared activity patterns locked to reward delivery. Notably, we found that it was substantially easier to distinguish the two populations in this 'frame of reference'; TR_D neurons showed a more robust and consistent modulation around reward (**Fig. 3a**). We quantified this by comparing the activity of pairs of neurons around task start and before reward. The peak modulation depth ratio for TR_D neurons around task start versus task end was significantly different (16.20 ± 0.96 versus 26.25 ± 1.24, respectively, paired *t* test, $t_{17} = -6.81$ $P < 10^{-5}$). On the other hand, the modulation depth of TR_I neurons did not significantly vary between the two frames of reference (13.84 ± 0.45 versus 12.86 ± 0.26, respectively, paired *t* test, $t_{104} = 1.95$, $P = 0.053$).

In general, we also noted that there was an apparent reduction in the variability of firing patterns for TR_D neurons as opposed to TR_I neurons associated with task completion. We quantified changes using the Fano factor (FF) method[35,36], which is a statistical measure of the trial-to-trial variability of neural firing. We found that TR_D neurons had the lowest FF at task end, which coincided with reward (**Fig. 3c**). These values were lesser than for task start of successful trials, and even lower than for task start of unsuccessful trials. Notably, when we matched for firing rates between the two frames using a subset of the neurons, we still observed the same decline in FF for the TR_D neurons in the task completion frame (TR_D neurons' FF: 0.37 ± 0.007 and 0.68 ± 0.016 for the task end and task start frames, respectively; TR_I neurons' FF: 0.71 ± 0.002 and 0.62 ± 0.002 for task end and task start, respectively; one-way ANOVA, $F_{5,350} = 41.20$, $P < 10^{-32}$). This suggests that the consistency of neural firing relative to reward may be an important determinant of rescaling.

To specifically dissociate task completion from reward, we performed 'variable reward' experiments ($BMI_{variable\text{-}reward}$) in which we uncoupled task completion from reward (**Fig. 3b**). This is contrasted from experiments that we outlined above in which the reward was delivered at a fixed interval after task completion ($BMI_{fixed\text{-}reward}$). More specifically, the water was delivered after a variable delay of 1–3 s after trial completion. Although the animals could learn the task (30.62 ± 6.47% improvement from BMI_{1Early} to BMI_{1Late}; paired *t* test, $t_3 = 4.46$, $P < 0.05$), we did not observe significant performance

gains from BMI_{1Late} to BMI_{2Early}, as typically seen in $BMI_{fixed\text{-}reward}$ trials (**Fig. 1c**). Notably, we also did not observe the rescaling effect; the change in modulation depth from BMI_{1Late} to BMI_{2Early} was 14.03 ± 7.89 and 3.35 ± 2.31% for TR_D and TR populations, respectively (paired *t* test, $t_5 = -1.95$, $P = 0.10$ for TR_D; $t_{40} = -1.46$, $P = 0.15$ for TR_I).

We then used these experiments to assess whether our observed changes were truly related to reward or simply task completion. For $BMI_{variable\text{-}reward}$ experiments, we no longer observed the reduction in FF for TR_D neurons at task completion (one-way ANOVA, $F_{3,166} = 83.86$, $P < 10^{-32}$, *post hoc t* test, $P < 0.05$; **Fig. 3c**). Moreover, they were indistinguishable from indirect neurons. Together, these data suggest that the lack of a temporally precise link between task completion and reward alters the differential modulation of the two populations previously seen. We then examined how the firing patterns of individual neurons changed for each of these two frames. We calculated the pairwise correlation between the sets of neurons during either trial start or trial end. Consistent with our hypothesis, the correlated firing between pairs of TR_D – TR_D and TR_D – TR_I neurons was significantly different for the reward-based frame for the $BMI_{fixed\text{-}reward}$ relative to the $BMI_{variable\text{-}reward}$ condition (pairwise correlation; one-way ANOVA, $F_{7,304} = 8.36$, $P < 10^{-8}$, *post hoc t* test, $P < 0.05$; **Fig. 4a**).

What is the effect of reward on reactivations? We found that neural co-firing in the reward frame could strongly predict the microstructure of reactivations for the $BMI_{fixed\text{-}reward}$ experiments ($R^2 = 0.54$, $P < 10^{-21}$; **Fig. 4b**); this relationship was not significant relative to task start (Spearman correlation, $r = 0.12$, $P = 0.19$) or for the $BMI_{variable\text{-}reward}$ experiments ($R^2 = 0.07$, $P > 0.05$; **Fig. 4c**). Taken together, our results indicate that firing patterns found in reactivation events are most closely related to the consistency of neural firing relative to the time of reward.

Closed-loop inhibition of spiking activity during slow oscillations

We next used closed-loop optogenetic methods to evaluate the causal role of the changes in sleep[37] functional connectivity in triggering both the offline performance gains and rescaling. We injected five rats with Jaws, a red-shifted halorhodopsin that is a potent silencer of neural activity[38]. After a period of several weeks, we performed a second surgery to implant microwire arrays attached to a cannula for fiber optic stimulation. The animals showed robust expression of Jaws and ~60% neurons responded to optical stimulation by reducing firing (~43% average reduction; **Fig. 5a–c**). Using each animal as its own control, we compared the effects of either allowing normal sleep ($n = 8$ sessions; $OPTO_{OFF}$) or conducting closed-loop perturbations ($n = 11$ sessions; $OPTO_{UP}$) to decouple spiking activity during UP states (that is, activated states hallmarked by neural firing during NREM sleep; **Fig. 5b**)[14,39]. We considered each session from a given animal as an independent observation. Optogenetic inhibition during $OPTO_{UP}$ experiments was specifically triggered during slow oscillations either by simple thresholding of filtered local field potential (LFP) during UP states ($n = 8$) or thresholding of power in the slow-wave band ($n = 3$; Online Methods). For the $OPTO_{DOWN}$ experiment, we exclusively used the filtered LFP to trigger the LED (**Fig. 5d**). These experiments were randomly interleaved among the animals. For the optogenetic experiments, we selected TR_D cells that responded to optical stimulation with reduced firing. **Figure 5b,c** shows examples of a TR_D neuron with normal firing during $Sleep_{pre}$ and suppressed firing during optogenetic stimulation linked to UP states ($Sleep_{post}$; population averages; **Fig. 5c**). The stimulation pulses during $OPTO_{UP}$ and $OPTO_{DOWN}$ experiments had similar incidences

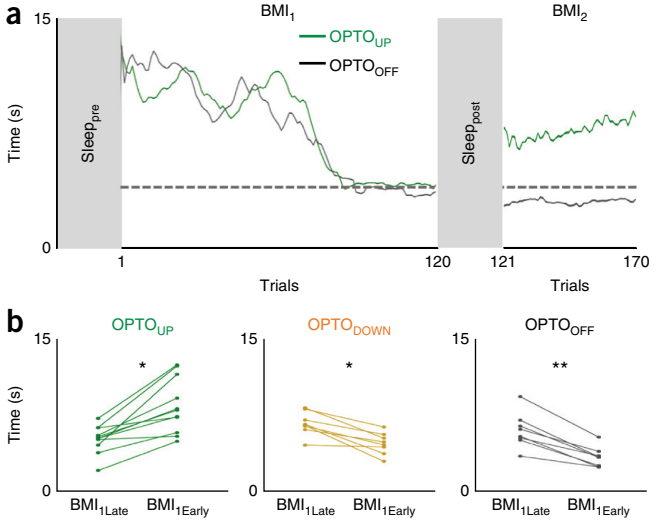

Figure 6 Optogenetic inhibition during UP states prevents consolidation. (**a**) Learning curves from two BMI sessions in the same rat with and without optogenetic inhibition during sleep (that is, $OPTO_{UP}$ and $OPTO_{OFF}$ sessions, respectively). (**b**) Performance changes from BMI_{1Late} to BMI_{2Early} in each of the three respective conditions ($OPTO_{UP}$ sessions paired *t* test $t_{10} = -5.52$, $^*P < 10^{-3}$; $OPTO_{DOWN}$ sessions paired *t* test $t_7 = 5.12$, $^*P < 10^{-3}$; $OPTO_{OFF}$ sessions paired *t* test $t_7 = 7.73$, $^{**}P < 10^{-4}$).

(**Supplementary Fig. 3a**) and proportion compared with total time spent in sleep (**Supplementary Fig. 3b**). All rats tolerated this manipulation without affecting total duration of sleep when compared with the $OPTO_{OFF}$ group (**Supplementary Fig. 4**). Furthermore, there were no quantitative changes in sleep power across the three conditions (**Fig. 5e,f**).

We observed significant worsening of performance only in the $OPTO_{UP}$ experiments (**Fig. 6a,b**). **Figure 6a** shows two examples of learning following pre- and post-sleep from two sessions in the same animal. Typically, we observed a worsening of performance relative to the end of the previous session in $OPTO_{UP}$ experiments, but the performance level was still better than that observed in the earliest trials. This was not the case with respective $OPTO_{DOWN}$ and $OPTO_{OFF}$ experiments. Taken together, these experiments suggest that decoupling of spiking during the UP states of slow oscillations is sufficient to prevent offline gains. This also strongly suggests that such a process is activity dependent and appears to at least require the local firing of action potentials during sleep. In addition, we also found that the performance worsening in BMI_2 in the $OPTO_{UP}$ experiments was associated with increased firing variability of TR_D neurons in both task-start and task-end frames of reference and was comparable to that of TR_I neurons (TR_D neuron FF: 1.04 ± 0.04 and 1.11 ± 0.08 at task end and task start, respectively; TR_I neuron FF: 1.07 ± 0.017 and 1.09 ± 0.02 at task end and task start, respectively; one-way ANOVA, $F_{3,220} = 0.44$, $P = 0.72$; $P > 0.05$ for all *post hoc* multiple comparisons). This was not the case after robust learning sessions in which TR_D neurons were associated with a significant reduction in FF at task end (**Fig. 3c**).

Optogenetic inhibition and rescaling

We next examined the extent of rescaling for the three experimental groups. Sessions with $OPTO_{UP}$ stimulation did not demonstrate rescaling of task activity in BMI_2, whereas the $OPTO_{DOWN}$ and $OPTO_{OFF}$ conditions resulted in the expected rescaling of TR_I neurons as previously observed (**Fig. 7a**). Furthermore, we evaluated neural dynamics

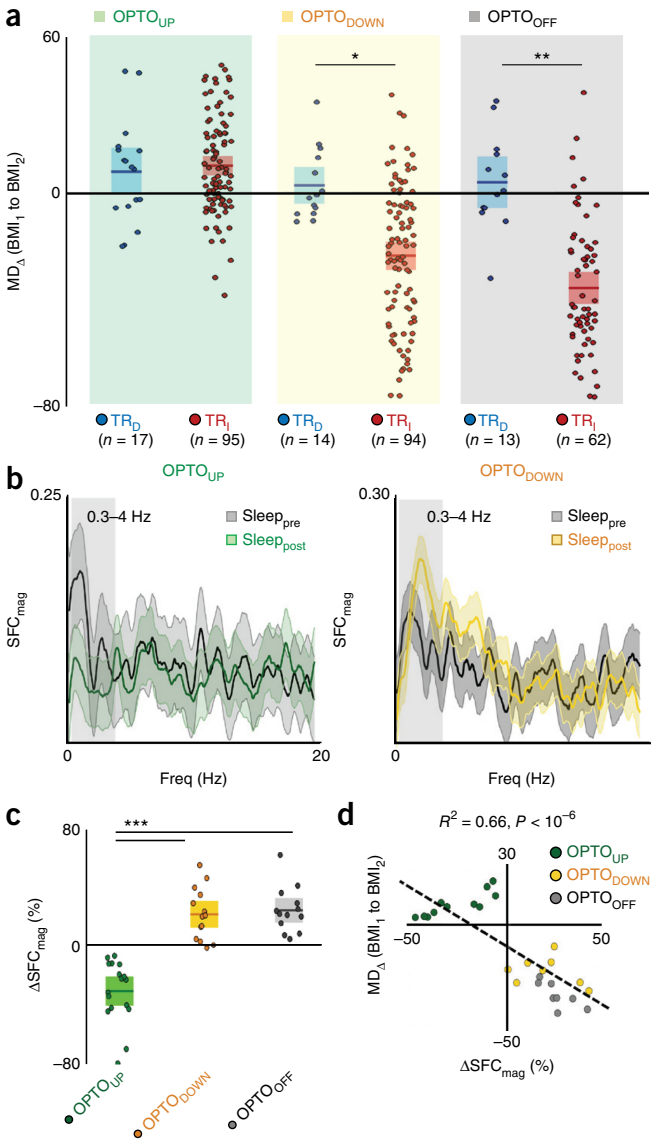

Figure 7 Optogenetic inhibition during UP states prevents rescaling of task activations. (**a**) Rescaling of TR_D and TR_I neurons measured through modulation depth change (MD_Δ) from BMI_1 and BMI_2 in $OPTO_{UP}$, $OPTO_{DOWN}$ and $OPTO_{OFF}$ experiments (mean in solid line ± s.e.m. in box; $OPTO_{UP}$ sessions unpaired *t* test $t_{110} = -0.47$, $P = 0.64$; $OPTO_{DOWN}$ sessions unpaired *t* test $t_{106} = 3.67$, $^*P < 10^{-3}$; $OPTO_{OFF}$ sessions paired *t* test $t_{73} = 5.52$, $^{**}P < 10^{-6}$). (**b**) Example plot of SFC as a function of frequency in $Sleep_{pre}$ and $Sleep_{post}$ in $OPTO_{UP}$ and $OPTO_{DOWN}$ experiment for two TR_D neurons. The lighter band is the jackknife error. (**c**) Averaged SFC changes from $Sleep_{pre}$ to $Sleep_{post}$ for TR_D neurons in $OPTO_{UP}$, $OPTO_{DOWN}$ and $OPTO_{OFF}$ groups (mean in solid line ± s.e.m. in box, one-way ANOVA, $F_{2,41} = 44.83$, $P < 10^{-10}$; significant *post hoc t* tests, $^{***}P < 0.05$). (**d**) Averaged SFC changes for TR_D cells versus averaged rescaling of TR_I cells from BMI_1 to BMI_2 in $OPTO_{UP}$, $OPTO_{DOWN}$ and $OPTO_{OFF}$ groups (linear regression $R^2 = 0.66$, $P < 10^{-6}$).

using spike-field coherence (SFC, see Online Methods regarding equalizing the number of spikes); SFC was significantly reduced for TR_I neurons from $Sleep_{pre}$ to $Sleep_{post}$ in the $OPTO_{UP}$ group (**Fig. 7b**,**c**). Finally, we also assessed whether the extent of the average SFC change (ΔSFC_{mag} from $Sleep_{pre}$ to $Sleep_{post}$) of TR_D neurons could predict the extent of the rescaling of TR_I neurons from BMI_1 to BMI_2 (MD_Δ). Notably, we found a significant relationship between changes in the SSC and the rescaling phenomenon ($R^2 = 0.66$, $P < 10^{-6}$; **Fig. 7d**). Together, these results suggest that our measured changes in sleep functional connectivity after learning may be required for the performance gains, the reduced variability of direct neurons and the rescaling of task-related activity.

DISCUSSION

In summary, we found evidence for rescaling of task-related neural activity after a period of NREM sleep. We specifically found selective downscaling of TR_I neural populations (that is, non-causal) in comparison with TR_D neurons (that is, causal) during task performance after NREM sleep. Our results further reveal how individual TR_D and TR_I neurons might be chosen for downscaling; we found that patterns of activity during sleep were predictive of task-related rescaling. During task practice, activity patterns that were most consistently related to rewarded outcomes matched the microstructure of reactivations. A more gross measure of neural firing linked to slow-oscillatory activity (that is, SSC in 0.3–4-Hz band) could also predict rescaling. Finally, we found that closed-loop optogenetic suppression of neural spiking during UP states prevented both performance gains and rescaling. Together, our results suggest that NREM sleep has an essential role in determining task-related functional connectivity that reflects the causal neuron behavior relationship. A net result of this process is to assign network credit assignment and to create sparser patterns of task-related activity.

Rescaling and sleep-dependent memory processing

Two commonly cited possibilities for the role of sleep in memory consolidation are a general strengthening of synaptic connectivity and a process of renormalization with net weakening of synaptic connectivity[12,14,18]. In the former, sleep is noted to have an active role in strengthening memories through enhanced local and distant connectivity, thereby resulting in systems consolidation. In contrast, in the latter, renormalization of synaptic strengths is believed to restore synaptic homeostasis and thereby benefit memory functions. It is worth noting that both processes could occur, but may operate over distinct timescales during long periods of sleep[14]. For example, recent evidence suggests that sleep is important for both pruning and growth of new spines[40–42]. Functionally, this could account for both the increases and decreases in neural firing after sleep[29]. Notably, a theoretical prediction is that synaptic renormalization may lead to rescaling of activity[18]; to the best of our knowledge there is no direct evidence of this. For natural learning, assessment of task-dependent renormalization is likely to be difficult given that the causality of neural activity to behavior is largely still unknown.

Neuroprosthetic learning allows us to readily distinguish neural activity that is causal for actuator movements (that is, TR_D) versus activity that is non-causal. Using this task, we found evidence of rescaling of task activity; specifically, that the task-related modulation of causal neurons were slightly, but significantly, enhanced, whereas non-causal neurons showed selective downscaling of task-related modulation. Although our specific experiments do not allow us to make conclusions regarding changes in synaptic strength, they do reveal that sleep-dependent processing can rescale task-dependent activations. At the very least, our results suggest that sleep-dependent processing does not exclusively strengthen functional connectivity, as assessed by task-related neural firing. Moreover, given that we also found a small, but significant, improvement in task performance as well as increased modulation of direct task-neurons, we cannot not exclude the possibility that a strengthening process may also simultaneously occur. Our experiments using optogenetic suppression of

spiking during the UP states suggests that our observed rescaling is driven by an activity-dependent process. Thus, our results also suggest that reactivations during sleep may be involved in a process of rescaling of task activity; this notion is also broadly consistent with predictions that renormalization may rely on the synchronous activity evident during slow oscillations[18].

Neuroprosthetic memory consolidation and slow oscillations

Our closed-loop optogenetic manipulation was triggered by phases of slow oscillations during sleep. We found that, although suppressing neural spiking during UP state (**Fig. 5b**,**d**) perturbed sleep-dependent effects, similar perturbations in the DOWN state did not have detectable effects. This suggests that the spontaneous reactivation of both task- and non-task-related neurons during UP states is required for sleep-dependent gains. Notably, our intervention did not appear to grossly affect sleep duration or the power spectrum of sleep. However, it is still possible that other known processes that are linked to slow oscillations might be involved. For example, it is known that spindles are associated with activity during UP states[13,14]. Although we did not detect gross changes in power, it is still possible that disruption of spiking during slow oscillations could affect spindles. Moreover, there is also a known link between cortical slow oscillations and hippocampal ripples[13,14]. Future studies can elucidate how other processes might contribute to consolidation after learning.

Our results further suggest that both performance gains and rescaling are regulated by spiking activity linked to slow oscillations. More specifically, NREM sleep appears to have a threefold effect on neural activity and performance. First, there was a significant effect of enhanced performance. Second, there was a slight, but significant, increase in the modulation depth of TR_D units. Finally, there was downscaling of TR_I activity. The latter two appear to be related to a rescaling effect in which the two populations are differentially modified. Our $OPTO_{UP}$ intervention affected both performance gains and the rescaling effect. Although it might seem that the modulation depth of TR_D units was still increased, we observed a significant increase in task-related variability for TR_D. Such enhanced variability may reflect poor consolidation of task-activity patterns and underlie the degradation of performance after the $OPTO_{UP}$ intervention. It can be likened to 'erosion' of memory, where rats forgot the neural activity pattern in BMI_1 and had to relearn the task again. Together, this suggests that rescaling of the two neural populations may occur simultaneously during UP states.

The SSC analysis shown in **Figure 2** suggests that the precise relationship between rescaling and SSC may be complex. There are at least three reasons why we measured a general increase in SSC in the setting of a largely selective enhancement of direct neurons. First, it is possible that there is an elevated threshold for plasticity. In other words, the intercept of our linear regression line suggests that the zero crossing (that is, the threshold for enhancement) is for values greater than a zero change in SSC. Second, it is possible that the general increase in SSC represents active processing of both populations during slow oscillations. In this view, the system might actively sample both weak and strong functional connectivity to ultimately determine credit assignment. Such active sampling would appear to result in a general increase in SSC. It is also worth noting that for hippocampal replay, there may be dissociation between the external experience and internal processing[43]. Thus, third, it is also possible that the elevated SSC represents a schema for internal representation that is not strictly related to the actual awake experience.

Our results might also suggest that both performance gains and rescaling are optimized by the same mechanisms. However, it is still possible that there is differential regulation of these two aspects of task performance. In both rodent and non-human primate models of neuroprosthetic learning, there is a dissociation between performance gains and rescaling[8,23]. For example, at the end of a typical practice session there were performance gains in the absence of rescaling (that is, firing of non-causal activity). Similarly, past work in non-human primates has indicated that rescaling can take days to occur, even in the presence of performance gains; the task used was substantially more complex than the one we used for rodents. This suggests that performance gains do not absolutely require rescaling. In our experiments, however, we found that sleep-dependent performance gains and rescaling were evident after a period of sleep. Moreover, disruption of spiking linked to slow oscillations resulted in both degradation of performance and rescaling. This suggests that sleep-dependent processing co-regulates both processes. However, given that sleep is a collection of heterogeneous and non-stationary phenomena[12,14], it is still quite possible that these two aspects can be dissociated. For example, our optogenetic intervention did not specifically examine the role of spindle activity that is coincident with slow oscillations (as opposed to all spiking linked to it). Future work can help to determine whether performance gains and rescaling are always co-regulated during sleep.

Role of reactivation in credit assignment

Our analysis specifically found that the timing of task activity relative to reward may determine credit assignment. Especially during 'early learning', co-firing of direct and indirect neurons occurred over multiple seconds. It is likely that the animals were exploring patterns of neural activity that could successfully complete the task. Notably, traditional task-related peri-event time histograms (PETHs) for neuroprosthetic performance are calculated on the basis of trial start; this is also typical for natural learning[31,35]. However, based on the extensive history on the role of reward in learning[32–34], we also examined PETHs that were associated with task end and reward delivery. Notably, the frame relative to reward was most predictive of rescaling and sleep-related reactivations. We also found that when we perturbed the link between reward and task completion (the variable reward experiments; **Figs. 3** and **4**) we no longer observed these phenomena. Together, these results are consistent with the growing notion that the patterns and extent of reward shapes learning and offline processing[10,44].

What might be a computational role for our observed rescaling of cortical activity and its association with reward? In general, reward-related reactivation may be a broad mechanism for learning and remembering experiences that lead to successful outcomes[32–34,45]. More specifically, the observed optimization of functional connectivity during sleep may provide important insight into the biological implementation of reinforcement learning, a widely studied theoretical and experimental model for reward-based learning[10,44]. In reinforcement learning, there is a noted tradeoff between exploration (gather new knowledge) versus exploitation (optimize decisions on the basis of current knowledge)[46]; it remains unclear how this is achieved precisely in biological systems. Our data suggests that sleep-dependent processing can allow for more targeted exploration on the basis of knowledge accumulated regarding reward-related neural firing during awake behaviors. Sleep may therefore allow further exploration of the statistics of the causal relation of neural activity to successful outcomes. The net result is the establishment of neural activity patterns that appear to reflect the causal neuron-behavior relationship.

METHODS

Methods, including statements of data availability and any associated accession codes and references, are available in the online version of the paper.

Note: Any Supplementary Information and Source Data files are available in the online version of the paper.

ACKNOWLEDGMENTS

This work was supported by awards from the Department of Veterans Affairs, Veterans Health Administration (VA Merit: 1I01RX001640 to K.G., VA CDA 1IK2BX003308 to D.S.R.); the National Institute of Neurological Disorders and Stroke (1K99NS097620 to T.G. and 5K02NS093014 to K.G.); the American Heart/Stroke Association (15POST25510020 to T.G.); the Burroughs Wellcome Fund (1009855 to K.G.); and start-up funds from the SFVAMC, NCIRE and UCSF Department of Neurology (to K.G.).

AUTHOR CONTRIBUTIONS

T.G. and K.G. conceived of the experiments. L.G. and T.G. performed surgical procedures and collected the data. A.B., D.S.R. and T.G. analyzed the data. T.G. and K.G. wrote the manuscript. L.G. and D.S.R. edited the manuscript.

COMPETING FINANCIAL INTERESTS

The authors declare no competing financial interests.

1. Yin, H.H. *et al.* Dynamic reorganization of striatal circuits during the acquisition and consolidation of a skill. *Nat. Neurosci.* **12**, 333–341 (2009).
2. Dayan, E. & Cohen, L.G. Neuroplasticity subserving motor skill learning. *Neuron* **72**, 443–454 (2011).
3. Tumer, E.C. & Brainard, M.S. Performance variability enables adaptive plasticity of 'crystallized' adult birdsong. *Nature* **450**, 1240–1244 (2007).
4. Shmuelof, L. & Krakauer, J.W. Are we ready for a natural history of motor learning? *Neuron* **72**, 469–476 (2011).
5. Peters, A.J., Chen, S.X. & Komiyama, T. Emergence of reproducible spatiotemporal activity during motor learning. *Nature* **510**, 263–267 (2014).
6. Ganguly, K. & Carmena, J.M. Emergence of a stable cortical map for neuroprosthetic control. *PLoS Biol.* **7**, e1000153 (2009).
7. Huber, D. *et al.* Multiple dynamic representations in the motor cortex during sensorimotor learning. *Nature* **484**, 473–478 (2012).
8. Ganguly, K., Dimitrov, D.F., Wallis, J.D. & Carmena, J.M. Reversible large-scale modification of cortical networks during neuroprosthetic control. *Nat. Neurosci.* **14**, 662–667 (2011).
9. Abbott, L.F., DePasquale, B. & Memmesheimer, R.M. Building functional networks of spiking model neurons. *Nat. Neurosci.* **19**, 350–355 (2016).
10. Lee, D., Seo, H. & Jung, M.W. Neural basis of reinforcement learning and decision making. *Annu. Rev. Neurosci.* **35**, 287–308 (2012).
11. Clancy, K.B., Koralek, A.C., Costa, R.M., Feldman, D.E. & Carmena, J.M. Volitional modulation of optically recorded calcium signals during neuroprosthetic learning. *Nat. Neurosci.* **17**, 807–809 (2014).
12. Tononi, G. & Cirelli, C. Sleep and the price of plasticity: from synaptic and cellular homeostasis to memory consolidation and integration. *Neuron* **81**, 12–34 (2014).
13. Diekelmann, S. & Born, J. The memory function of sleep. *Nat. Rev. Neurosci.* **11**, 114–126 (2010).
14. Genzel, L., Kroes, M.C., Dresler, M. & Battaglia, F.P. Light sleep versus slow wave sleep in memory consolidation: a question of global versus local processes? *Trends Neurosci.* **37**, 10–19 (2014).
15. Cramer, S.C. *et al.* Motor cortex activation is preserved in patients with chronic hemiplegic stroke. *Ann. Neurol.* **52**, 607–616 (2002).
16. Marshall, L. & Born, J. The contribution of sleep to hippocampus-dependent memory consolidation. *Trends Cogn. Sci.* **11**, 442–450 (2007).
17. Wilson, M.A. & McNaughton, B.L. Reactivation of hippocampal ensemble memories during sleep. *Science* **265**, 676–679 (1994).
18. Nere, A., Hashmi, A., Cirelli, C. & Tononi, G. Sleep-dependent synaptic down-selection (I): modeling the benefits of sleep on memory consolidation and integration. *Front. Neurol.* **4**, 143 (2013).
19. Jarosiewicz, B. *et al.* Functional network reorganization during learning in a brain-computer interface paradigm. *Proc. Natl. Acad. Sci. USA* **105**, 19486–19491 (2008).
20. Koralek, A.C., Jin, X., Long, J.D. II, Costa, R.M. & Carmena, J.M. Corticostriatal plasticity is necessary for learning intentional neuroprosthetic skills. *Nature* **483**, 331–335 (2012).
21. Taylor, D.M., Tillery, S.I. & Schwartz, A.B. Direct cortical control of 3D neuroprosthetic devices. *Science* **296**, 1829–1832 (2002).
22. Moritz, C.T., Perlmutter, S.I. & Fetz, E.E. Direct control of paralyzed muscles by cortical neurons. *Nature* **456**, 639–642 (2008).
23. Gulati, T., Ramanathan, D.S., Wong, C.C. & Ganguly, K. Reactivation of emergent task-related ensembles during slow-wave sleep after neuroprosthetic learning. *Nat. Neurosci.* **17**, 1107–1113 (2014).
24. Gulati, T. *et al.* Robust neuroprosthetic control from the stroke perilesional cortex. *J. Neurosci.* **35**, 8653–8661 (2015).
25. Fetz, E.E. Volitional control of neural activity: implications for brain-computer interfaces. *J. Physiol. (Lond.)* **579**, 571–579 (2007).
26. Koralek, A.C., Costa, R.M. & Carmena, J.M. Temporally precise cell-specific coherence develops in corticostriatal networks during learning. *Neuron* **79**, 865–872 (2013).
27. Orsborn, A.L. *et al.* Closed-loop decoder adaptation shapes neural plasticity for skillful neuroprosthetic control. *Neuron* **82**, 1380–1393 (2014).
28. Mitchell, J.F., Sundberg, K.A. & Reynolds, J.H. Spatial attention decorrelates intrinsic activity fluctuations in macaque area V4. *Neuron* **63**, 879–888 (2009).
29. Watson, B.O., Levenstein, D., Greene, J.P., Gelinas, J.N. & Buzsáki, G. Network homeostasis and state dynamics of neocortical sleep. *Neuron* **90**, 839–852 (2016).
30. Peyrache, A., Khamassi, M., Benchenane, K., Wiener, S.I. & Battaglia, F.P. Replay of rule-learning related neural patterns in the prefrontal cortex during sleep. *Nat. Neurosci.* **12**, 919–926 (2009).
31. Ramanathan, D.S., Gulati, T. & Ganguly, K. Sleep-dependent reactivation of ensembles in motor cortex promotes skill consolidation. *PLoS Biol.* **13**, e1002263 (2015).
32. Lansink, C.S., Goltstein, P.M., Lankelma, J.V., McNaughton, B.L. & Pennartz, C.M. Hippocampus leads ventral striatum in replay of place-reward information. *PLoS Biol.* **7**, e1000173 (2009).
33. de Lavilléon, G., Lacroix, M.M., Rondi-Reig, L. & Benchenane, K. Explicit memory creation during sleep demonstrates a causal role of place cells in navigation. *Nat. Neurosci.* **18**, 493–495 (2015).
34. Singer, A.C. & Frank, L.M. Rewarded outcomes enhance reactivation of experience in the hippocampus. *Neuron* **64**, 910–921 (2009).
35. Churchland, M.M. *et al.* Stimulus onset quenches neural variability: a widespread cortical phenomenon. *Nat. Neurosci.* **13**, 369–378 (2010).
36. Song, W. & Giszter, S.F. Adaptation to a cortex-controlled robot attached at the pelvis and engaged during locomotion in rats. *J. Neurosci.* **31**, 3110–3128 (2011).
37. Miyamoto, D. *et al.* Top-down cortical input during NREM sleep consolidates perceptual memory. *Science* **352**, 1315–1318 (2016).
38. Chuong, A.S. *et al.* Noninvasive optical inhibition with a red-shifted microbial rhodopsin. *Nat. Neurosci.* **17**, 1123–1129 (2014).
39. Steriade, M., Nuñez, A. & Amzica, F. A novel slow (<1 Hz) oscillation of neocortical neurons in vivo: depolarizing and hyperpolarizing components. *J. Neurosci.* **13**, 3252–3265 (1993).
40. Yang, G. *et al.* Sleep promotes branch-specific formation of dendritic spines after learning. *Science* **344**, 1173–1178 (2014).
41. de Vivo, L. *et al.* Ultrastructural evidence for synaptic scaling across the wake/sleep cycle. *Science* **355**, 507–510 (2017).
42. Maret, S., Faraguna, U., Nelson, A.B., Cirelli, C. & Tononi, G. Sleep and waking modulate spine turnover in the adolescent mouse cortex. *Nat. Neurosci.* **14**, 1418–1420 (2011).
43. Gupta, A.S., van der Meer, M.A., Touretzky, D.S. & Redish, A.D. Hippocampal replay is not a simple function of experience. *Neuron* **65**, 695–705 (2010).
44. O'Doherty, J.P., Cockburn, J. & Pauli, W.M. Learning, reward, and decision making. *Annu. Rev. Psychol.* **68**, 73–100 (2017).
45. Schultz, W. Behavioral theories and the neurophysiology of reward. *Annu. Rev. Psychol.* **57**, 87–115 (2006).
46. Ishii, S., Yoshida, W. & Yoshimoto, J. Control of exploitation-exploration meta-parameter in reinforcement learning. *Neural Netw.* **15**, 665–687 (2002).

ONLINE METHODS

Animals/surgery. Experiments were approved by the Institutional Animal Care and Use Committee at the San Francisco VA Medical Center. We used a total of ten adult Long-Evans male rats (n = 5 were used for optogenetic experiments). No statistical methods were used to pre-determine sample sizes, but our sample sizes are similar to those reported in previous publications[23,31]. Animals were kept under controlled temperature and a 12-h light: 12-h dark cycle with lights on at 06:00 a.m. Probes were implanted during a recovery surgery performed under isofluorane (1–3%) anesthesia. Atropine sulfate was also administered before anesthesia (0.02 mg/kg of body weight) The post-operative recovery regimen included administration of buprenorphine at 0.02 mg/kg and meloxicam at 0.2 mg/kg . Dexamethasone at 0.5 mg/kg and Trimethoprim sulfadiazine at 15 mg/kg were also administered post-operatively for 5 d. We used 32-channel microwire arrays; arrays were lowered down to 1,400–1,800 μm in the primary motor cortex (M1) in the upper limb area (1–3 mm anterior to bregma and 2–4 mm lateral from midline). The reference wire was wrapped around a screw inserted in the midline over the cerebellum. Final localization of depth was based on quality of recordings across the array at the time of implantation. All animals were allowed to recover for 1-week before start of experiments. Data collection and analysis were not performed blind to the conditions of the experiments.

Viral injections. We used a red-shifted halorhodopsin, Jaws (AAV8-hSyn-Jaws-KGC-GFP-ER2, UNC Viral Core) for neural silencing in 5 rats for optogenetic experiments[38]. Viral injections were done at least 2.5 weeks before chronic microelectrode array implant surgeries. Rats were anesthetized, as stated before and body temperature was maintained at 37 °C with a heating pad. Burr hole craniotomies were performed over injection sites, and the virus was injected using a Hamilton Syringe with 34G needle. 500-nl injections (100 nl per min) were made into deep cortical layers (1.4 mm from surface of brain) at two sites in M1 (coordinates relative to bregma: posterior, 0.5 mm and lateral, 3.5 mm; and anterior, 1.5 mm and lateral, 3.5 mm). After the injections, the skin was sutured and the animals were allowed to recover with same regimen as stated above. Viral expression was confirmed with fluorescence imaging. Optogenetic inhibition significantly reduced firing in M1 neurons, with a reduction in 50–70% of recorded cells.

Electrophysiology. We recorded extracellular neural activity using tungsten microwire electrode arrays (MEAs, Tucker-Davis Technologies (TDT)). We recorded spike and LFP activity using a 128-channel TDT-RZ2 system (TDT). Spike data was sampled at 24,414 Hz and LFP data at 1,018 Hz. ZIF-clip-based analog headstages with a unity gain and high impedance (~1 G) was used. Optogenetic experiments, including controls, were done with digital headstages primarily because of the ability to pass the optical fiber through the commutator. Only clearly identifiable units with good waveforms and high signal-to-noise ratio were used. The remaining neural data was recorded for offline analysis. Behavior related timestamps (that is, trial onset, trial completion) were sent to the RZ2 analog input channel using a digital board and synchronized to neural data. We initially used an online sorting program (SpikePac, TDT) for neuroprosthetic control. We then conducted offline sorting[23].

Behavior. After recovery, animals were typically handled for several days before the start of experimental sessions. Animals acclimated to a custom plexiglass behavioral box (**Fig. 1a**) during this period. The box was equipped with a door at one end. Initially, water delivery from the actuator was not introduced and they were just acclimatized to the box. Toward the end of the acclimation period, the rats typically fell asleep while in the box. Animals were then water scheduled such that water (from the feeding tube illustrated in **Fig. 1a**) was available in a randomized fashion while in the behavioral box. We monitored body weights on a daily basis to ensure that the weight did not drop below 95% of the initial weight. Behavioral sessions were conducted in the morning, with second sessions conducted in the afternoon. We recorded neural data from the rats for 2 h before start of BMI training (that comprised $Sleep_{pre}$). The rats were then allowed to perform the task over a ~2-h session (BMI_1). Recorded neural data was entered in real-time from the TDT workstation to custom routines in Matlab. These then served as control signals for the angular velocity of the feeding tube. The rats typically performed ~180–200 trials per session. These sessions typically lasted from 90–120 min based on the rate of trial completion. Following this, we recorded neural data from animals for a 2-h period (including $Sleep_{post}$). The animals then continued with another 90–120-min training session (BMI_2). Sorted units at the beginning of the recording were checked for maintenance throughout the second training session.

Neural control of the feeding tube. During the BMI training sessions, we typically randomly selected two well–isolated units as 'direct' and allowed their neural activity to control the angular velocity of the feeding tube. In two of the ten sessions (that is, from the 5 non-viral injected rats), there was only one neuron selected as the direct unit. The remaining neurons in all the experiments (that is, indirect) were recorded but not causally linked to actuator movements. We did not find any systematic differences in waveform shape (that is, narrow versus broad) or baseline firing rate for these two populations. These units maintained their stability throughout the recording as evidenced by stability of waveform shape and interspike–interval histograms. We binned the spiking activity into 100-ms bins. We then established a mean firing rate for each neuron over a 3–5-min baseline period. During this period the animals were typically transitioning between walking, exploring and periods of rest.

The mean firing rate was then subtracted from its current firing rate at all times. The specific transform that we used was

$$\theta_v = C * (G_1 * r_1(i) + G_2 * r_2(i))$$

where θ_v was the angular velocity of the feeding tube, $r_1(i)$ and $r_2(i)$ were firing rates of the direct units. G_1 and G_2 were randomized coefficients that ranged from +1 to −1 and were held constant after initialization. C was a fixed constant that scaled the firing rates to arrive at a value for angular velocity. The animals were then allowed to control the feeding tube via modulation of neural activity. The tube started at the same position at the start of each trial (P_1 in **Fig. 1a**,**b**). The calculated angular velocity was added to the previous angular position at each time step (100 ms). During each trial, the angular position could range from −45 to +180 degrees. If the tube stayed in the 'target zone' (P_2 in **Fig. 1a**; spanned 10° area) for a period of 300 ms, a water reward was delivered. In the $BMI_{variable\text{-}reward}$ experiments (n = 4 sessions in two rats), the rats correctly positioned the tube, but reward delivery (that is, the water from the tube) was randomly delayed by a period ranging from 1–3 s. In contrast, the $BMI_{fixed\text{-}reward}$ (that is, typical BMI session), the reward was delivered with a fixed delay of ~200 ms relative to task completion. In the beginning of a session, most rats were unsuccessful at bringing the feeding tube to position P_2. Most rats steadily improved control and reduced the time to completion of the task during the first session. We obtained multiple learning sessions from each animal. These sessions were typically several days to 1 week apart to ensure that new units were recorded. Consistent with past studies, we also found that incorporation of new units into the control scheme required new learning[8,23].

Closed-loop sleep experiments using optogenetics. Three types of experiments were conducted using the five Jaws-injected animals, namely $OPTO_{UP}$ (n = 11), $OPTO_{DOWN}$ (n = 8) and $OPTO_{OFF}$ (n = 8). These experiments were largely randomly interspersed among the animals. However, while the $OPTO_{DOWN}$ were only conducted in three animals, these animals also contributed to the $OPTO_{UP}$ and $OPTO_{OFF}$ experiments. In general, we identified the phases of the LFP associated with 'UP' and 'DOWN' states based on the relationship of the neural spiking to the LFP. For example, as shown in **Figure 5**, the negativity in our LFP signals was associated with neural spiking and thus consistent with an UP state, which are natural states of increased activity during slow oscillations.

The closed-loop interventions were conducted by triggering the LED light based on real-time detection of cortical states. We used a custom script in the RPvdsEx Prgram (TDT) to identify slow oscillations in real-time during sleep blocks. In the $OPTO_{UP}$ experiments, we conducted two types of triggering (n = 3 power based; n = 8 filtering based). In both cases, the LED light was delivered during cortical 'UP' states by placing a manual threshold on filtered LFP trace; the manual threshold was selected visually to coincide with the respective phase on the slow oscillations as noted below. For the 'power-based' triggering, we used the following approach. The algorithm/workstation calculated the LFP power in the 0.1–4-Hz range and compared it to the threshold. Once the threshold was exceeded for >100 ms, LED illumination (625-nm fiber-coupled LED

(ThorLabs)), with 200/400-μm diameter optic fibers (Doric Lenses) was triggered for 100 ms. For the 'filtering based' approach, we used a real-time implementation of a Butterworth filter to filter the raw LFP in a 0.1–4-Hz band (**Fig. 5d**). The UP state was determined by setting a 'negative' threshold on the LFP (that is, as displayed in the convention in **Fig. 5d**). The LED was again triggered when it was respectively above/below this threshold. Notably, this type of stimulation was exclusive to the UP state. Because we did not observe any differences we combined both sets as the $OPTO_{UP}$ condition.

During $OPTO_{DOWN}$ sessions, we directly placed a 'positive' threshold on the filtered LFP; thus the stimulation was triggered during threshold crossings of 'DOWN' (that is, DOWN states with natural periods of quiescence during slow oscillations). These stimulations were also typically brief (that is, 100 ms). A typical example is shown in **Figure 5**. **Supplementary Figure 3** shows that total incidents of 100-ms stimulations were similar in both $OPTO_{UP}$ and $OPTO_{DOWN}$ experiments, and the light was on for a similar proportion of time. Finally, a group of control experiments called $OPTO_{OFF}$ (that is, where no stimulation was triggered) was also conducted in the Jaws-injected rats. Durations of total pre and post sleep were similar in all 3 session types (**Supplementary Fig. 4**). We also calculated LFP power and SFC changes for individual neurons in all three groups.

Sessions and changes in performance. Analysis was performed in Matlab (Mathworks) with custom-written routines. A total of ten $BMI_{fixed\text{-}reward}$ training sessions recorded from five rats were used for our initial analysis. All of these sessions demonstrated 'robust learning' (that is, >3 s.d. drop in time to completion in the last 1/3 of trials or 'late' trials in comparison to the first 1/3 of trials or 'early' trials). These sessions were followed by a second training session (that is, BMI_2). In **Figure 1c**, we compared changes in task performance across sessions. Specifically, we compared the performance change between BMI_{1Late}, BMI_{2Early} and BMI_{2Late} by calculating the mean and standard error of the time to completion during the last third trials in BMI_1 and the first and last third trials BMI_2 (**Fig. 1c**). We used a paired *t* test to assess statistical significance.

Task-related activity. The distinction between TR_D and TR_I neurons was based on whether units were used for the direct neural control of the feeding tube. The change in modulation depth (MD_Δ) was calculated by comparing the peak activity around the task (in the 5-s window after the task start/ 4 s before task-end/reward) over baseline firing activity (averaged activity of 4 s before task start) on the peri-event time histograms (PETH, bin length 50 ms). In other words, the MD_Δ is a measure of the modulation of firing rate relative to the pre-task start baseline rate. Modulation of baseline firing activity after the 'Go cue' (task start) or before receipt of 'reward' (task end) was calculated and this was compared for TR_D and TR_I neurons from BMI_1 to BMI_2 (MD_Δ change from BMI_1 to BMI_2). This was calculated across the last third of trials from BMI_1 and first and last third of trials from BMI_2 (BMI_{2Early} and BMI_{2Late} respectively). In a BMI session with approximately 200 trials, these values were averaged across ~65 trials. To ensure that any online training effects were not contributing to the observed reduction in MD_Δ of TR_I units, in a subset of these sessions we also averaged MD_Δ for just 30 trials before and after; no significant differences were evident.

For **Figures 1** and **3**, PETH were smoothed using a Bayesian adaptive-regression spline algorithm, implemented within MATLAB using toolboxes downloaded at (http://www.cnbc.cmu.edu/~rkelly/code.html)[31,47]. The algorithm automatically optimized for the number and location of 'knots' (that is, regions in which a new local regression model improves the overall fit of the curve) was determined automatically using a Markov chain Monte Carlo implemented to optimize the Bayes Information Criteria and thereby, offered a better visualization of dynamic changes in the rate of change of spike trains. These curves were not used for other sets of analysis.

Identification of NREM oscillations. Identification of pre- and post-NREM epochs was performed by combined visual assessment of presence of low-frequency, high-amplitude slow-wave oscillations as well as a 3 s.d. threshold of the filtered data (0.3–4 Hz). If there was a sustained reduction >1.5 s in the amplitude of the slow-wave activity below threshold during a continuous epoch we excluded these segments[23,31].

Coherency measure. We used the Chronux toolbox to calculate the SSC (http://chronux.org/)[48]. Its magnitude is a function of frequency and takes values between 0 and 1. For its calculation, the pre- and post-sleep were segmented into 20-s segments and then the coherency measured was averaged across segments. For the multitaper analysis, we used a time-bandwidth (TW) product of 10 with 19 tapers. To compare coherences across groups, a *z* score was calculated using the programs available in the Chronux Toolkit. Coherence between activity in two regions, C_{xy} was calculated and defined as

$$C_{xy} = \frac{|R_{xy}|}{\sqrt{R_{xx}}\sqrt{R_{yy}}}$$

where R_{xx} and R_{yy} are the power spectra and R_{xy} is the cross-spectrum. More specifically, it is a pairwise measure of synchronized co-firing of neurons in a frequency dependent manner. For example, during NREM sleep, it can quantify synchronous co-firing relative to low-frequency oscillations in the 0.3–4-Hz range. Our previous work has also shown that SSC values are related to the spike cross-correlogram measured during UP states[23].

Spectral analysis were calculated in segmented NREM epochs and averaged across these epochs across animals. Mean coherence was calculated between 0.3–4 Hz. Significance testing on coherence estimates was performed on mean estimates between TR_D – TR_D and TR_D – TR_I pairs using unpaired *t* tests. The task-related direct unit with the greatest depth modulation was used to calculate SSC for every other unit. Similarly, for SFC analysis in optogenetic experiments, mean power changes in the 0.3–4-Hz band were compared for $OPTO_{UP}$; $OPTO_{DOWN}$ and $OPTO_{OFF}$ experiments. We also equaled the number of spikes in pre- and post-sleep[23,28] to account for the changes in firing rates; this was especially pertinent for the optogenetic intervention studies.

Ensemble activation analyses. To characterize ensemble reactivations following sleep, we performed an analysis that compared neural activity patterns during $Sleep_1$ and $Sleep_2$ with a template that was created during task execution in BMI_1[23,30,31]. We first computed a pairwise unit activity correlation matrix during BMI_1 by concatenating binned spike trains (t_{bin} = 50 ms) for each neuron across trials (0.5 s before the onset of trial up to 5s after the onset of BMI task for each trial). This concatenated spike train was z-transformed, and then organized into a 2-D matrix organized by neurons (x) and time (B for number of time bins). From this spike count matrix, we calculated the correlation matrix (C_{task}), and then calculated the eigenvector for the largest eigenvalue from this correlation matrix to study. This eigenvector was used as the ensemble template of activity, which was then projected back on to the neural activity trains from the same population of neurons during $Sleep_1$ and $Sleep_2$. This projection was a linear combination of Z-scored binned neural activity from the two blocks above, weighted by the PC ensemble (that is, the eigenvector) calculated from the BMI_1 matrix. This linear combination has been described as the "activation strength" of that particular ensemble. In this analysis we focused on the first eigenvector, as the first PC explained most task-related variance (see **Supplementary Fig. 5** for two examples).

Reactivation triggered peri-event time histogram (microstructure of reactivation). We also constructed time histograms of single unit activity around reactivation events. We binned spike counts from 250 ms before and after ensemble reactivation events using a 5-ms bin size and calculated the mean/standard error of the binned neural firing. The reactivation events that were chosen for PETHs were those with a reactivation strength that was significantly greater than for the pre- sleep block. Usually top 10–20 percentile reactivation strengths from the post-sleep fulfilled this criterion. Once the PETHs were constructed, the modulation depth around reactivations ($MD_{reactivation}$) was calculated by comparing the peak of firing during reactivation to the mean baseline firing (that is, at the tails). *t* test was performed to compare $MD_{reactivation}$ between TR_D and TR_I units, and also their levels in pre-sleep. We also checked for $MD_{reactivation}$ of TR_D and TR_I units at random low-percentile reactivation events and their $MD_{reactivation}$ was indistinguishable (**Supplementary Fig. 1**).

Analyses of neural firing variability and neuronal pair correlations. The modulation characteristics of each neuron in the BMI task in the two frames of reference (namely, 'task-start' and 'task-end') were examined using the following: Fano factor, which is a statistical measure of the dynamics of the firing rate of

doi:10.1038/nn.4601

a cell[35,36]; and cross-correlation calculated between the rates of cell pairs. Fano factor, F is defined as

$$F = \frac{\sigma^2}{\mu}$$

where σ^2 is the variance and μ is the mean of a spike count process (here in a 50-ms time window). μ was the average firing rate and was calculated as follows:

$$\mu = \frac{1}{B} \sum_{n=1:B} C(n)$$

where $C(n)$ is the spike counts in 50-ms time window and B is the total window sample number. Since, fano factor can be influenced by firing rate, we also compared fano factor in task start and task end frames of reference where the firing rates were similar and we still found similar trends. Cross-correlation, on the other hand, measured the similarity of two firing rate series (50-ms bins) as a function of the displacement of one relative to the other. This pairwise correlation of the neural activity was calculated for TR_D – TR_D and TR_D – TR_I neuronal pairs using Matlab's *xcorr* function (**Fig. 4**). Time series of concatenated binned spike counts were created either around task start (first 1 s) or around task end (from trial end to 1 s prior). Statistical comparisons were performed using a repeated-measures ANOVA, followed by *post hoc t* tests to identify specific time points that were significantly different.

Statistics. There were a total of 10 robust BMI learning sessions that we used ($BMI_{fixed\text{-}reward}$) for analyzing the trends from BMI_1 to BMI_2. There were a total of 18 TR_D and 105 TR_I units in these experiments. There were also 4 $BMI_{variable\text{-}reward}$ sessions where we had 6 TR_D and 41 TR_I neurons. Optogenetics experiments (in Jaws-injected rats) had 11 sessions with $OPTO_{UP}$ stimulation (with 17 TR_D and 95 TR_I units), 8 sessions with $OPTO_{DOWN}$ stimulation (with 14 TR_D and 94 TR_I units), and 8 sessions with $OPTO_{OFF}$ stimulation (with 13 TR_D and 62 TR_I units). We also recorded sleep before ($Sleep_{pre}$) and after ($Sleep_{post}$) after BMI_1. In all these experiments, we performed paired *t*-test to compare performance changes from BMI_1 to BMI_2 ; MD_Δ change for TR_D or TR_I units from BMI_1 to BMI_2; $MD_{reactivation}$ change and firing rate changes for TR_D and TR_I units from $Sleep_{pre}$ to $Sleep_{post}$; SSC_{mag} changes for TR_D – TR_D and TR_D – TR_I neuronal pairs from $Sleep_{pre}$ to $Sleep_{post}$ (**Figs. 1c** and **6b**). Data distribution was tested for normality and non-parametric test was substituted if needed (Wilcoxon signed rank test). Unpaired *t* tests were also used for comparisons such as $MD_{reactivation}$ in TR_D versus TR_I units pools; MD_Δ change for TR_D versus TR_I units from BMI_1 and BMI_2; and features of stimulation in $OPTO_{UP}$ and $OPTO_{DOWN}$ experiments (**Figs. 1e** and **7a**; **Supplementary Figs. 1** and **3**). We also performed one-way ANOVA with multiple comparisons (test of homogeneity of variances was done) wherever significance assessment was required (**Figs. 2e**, **3c**, **4a**, **5c**,**f** and **7c**, and **Supplementary Fig. 4**). We also used linear regression or correlation to evaluate trends between $MD_{reactivation}$ versus MD_Δ change from BMI_1 and BMI_2, or correlated firing around task start or task end; pairwise firing correlation of TR_D – TR_D and TR_D – TR_I neuronal pairs versus $MD_{reactivation}$; between time spent in NREM sleep and MD_Δ change from BMI_1 and BMI_2 for different units; and SSC_{mag} changes for TR_D – TR_D and TR_D – TR_I neuronal pairs versus MD_Δ change for TR_D or TR_I units from BMI_1 to BMI_2; and SFC changes in optogenetics experiments, versus MD_Δ change (**Figs. 2b**, **4b**,**c** and **7d**, and **Supplementary Fig. 2**).

A **Supplementary Methods Checklist** is available.

Data availability statement. The data that support the findings from this study are available from the corresponding author upon request.

47. Wallstrom, G., Liebner, J. & Kass, R.E. An implementation of Bayesian adaptive regression splines (BARS) in C with S and R Wrappers. *J. Stat. Softw.* **26**, 1–21 (2008).
48. Mitra, P. & Bokil, H. *Observed Brain Dynamics* (Oxford University Press, 2008).

nature neuroscience

Corresponding Author: Karunesh Ganguly, MD PhD

Manuscript Number: NN-BC54927A-Z

Manuscript Type: Article

Main Figures: 7

Supplementary Figures: 5

Supplementary Tables: 0

Supplementary Videos: 0

Reporting Checklist for Nature Neuroscience

This checklist is used to ensure good reporting standards and to improve the reproducibility of published results. For more information, please read Reporting Life Sciences Research.

Please note that in the event of publication, it is mandatory that authors include all relevant methodological and statistical information in the manuscript.

Statistics reporting, by figure

- Please specify the following information for each panel reporting quantitative data, and where each item is reported (section, e.g. Results, & paragraph number).
- Each figure legend should ideally contain an exact sample size (n) for each experimental group/condition, where n is an exact number and not a range, a clear definition of how n is defined (for example x cells from x slices from x animals from x litters, collected over x days), a description of the statistical test used, the results of the tests, any descriptive statistics and clearly defined error bars if applicable.
- For any experiments using custom statistics, please indicate the test used and stats obtained for each experiment.
- Each figure legend should include a statement of how many times the experiment shown was replicated in the lab; the details of sample collection should be sufficiently clear so that the replicability of the experiment is obvious to the reader.
- For experiments reported in the text but not in the figures, please use the paragraph number instead of the figure number.

Note: Mean and standard deviation are not appropriate on small samples, and plotting independent data points is usually more informative. When technical replicates are reported, error and significance measures reflect the experimental variability and not the variability of the biological process; it is misleading not to state this clearly.

		TEST USED		n			DESCRIPTIVE STATS (AVERAGE, VARIANCE)		P VALUE		DEGREES OF FREEDOM & F/t/z/R/ETC VALUE	
	FIGURE NUMBER	WHICH TEST?	SECTION & PARAGRAPH #	EXACT VALUE	DEFINED?	SECTION & PARAGRAPH #	REPORTED?	SECTION & PARAGRAPH #	EXACT VALUE	SECTION & PARAGRAPH #	VALUE	SECTION & PARAGRAPH #
example	1a	one-way ANOVA	Fig. legend	9, 9, 10, 15	mice from at least 3 litters/group	Methods para 8	error bars are mean +/- SEM	Fig. legend	p = 0.044	Fig. legend	F(3, 36) = 2.97	Fig. legend
example	results, para 6	unpaired t-test	Results para 6	15	slices from 10 mice	Results para 6	error bars are mean +/- SEM	Results para 6	p = 0.0006	Results para 6	t(28) = 2.808	Results para 6
+ -	1c	paired t-test	Results , Para1	10	10 BMI1 and BMI2 sessions	Results, Para1	error bars are mean +/- SEM	Fig. 1 legend	3.2320e-05	Results, Para2	t(9)=7.62	Results, Para2

		TEST USED		n			DESCRIPTIVE STATS (AVERAGE, VARIANCE)		P VALUE		DEGREES OF FREEDOM & F/t/z/R/ETC VALUE	
	FIGURE NUMBER	WHICH TEST?	SECTION & PARAGRAPH #	EXACT VALUE	DEFINED?	SECTION & PARAGRAPH #	REPORTED?	SECTION & PARAGRAPH #	EXACT VALUE	SECTION & PARAGRAPH #	VALUE	SECTION & PARAGRAPH #
+ -	1e	upaired t-test	Results, Para2	TRd=18, TRi=105	Modulation depth change from BMI1 to BMI2 early trials	Results, Para2	box plot with mean +/- SEM	Fig 1 legend	4.4679e-10	Fig 1 legend	t(121)=6.7891	Results, Para2
+ -	1e	upaired t-test	Results, Para2	TRd=18, TRi=105	Modulation depth change from BMI1 to BMI2 late trials	Results, Para2	box plot with mean +/- SEM	Fig 1 legend	4.6799e-09	Fig 1 legend	t(121)=6.3138	Results, Para2
+ -	1e	upaired t-test	Results, Para2	TRd=18, TRi=105	Modulation depth change from BMI1 to all BMI2 trials	Results, Para2	box plot with mean +/- SEM	Fig 1 legend	1.8915e-10	Fig 1 legend	t(121)=6.9596	Results, Para2
+ -	NA	unpaired t-test	Results, Para3	TRd-TRd=8, TRd-TRi=105	SSC change for TRd-TRd and TRd-TRi pairs	Results, Para3	box plot with mean +/- SEM	Results, Para3	1.4856e-08	Results, Para3	t(121)=6.074	Results, Para3
+ -	2b	pearson correlation	Results, Para3	228	SSC vs modulation depth changes for TRd and TRiunits from BMI1 to BMI2	Results, Para3	correlation	Fig 2, legend	P<0.05	Fig 2 legend	r(123)=0.51	Results, Para3
+ -	2e	one-way ANOVA	Results, Para6	TRd=18 +18, TRi=105 +105 (Pre and post sleep)	Modulation during reactivation for TRd and TRi from pre sleep to post sleep	Results, Para6	box plot with mean +/- SEM	Fig 2 legend	1.6837e-18	Fig 2 legend	F(3,242)=34.28	Results, Para6
+ -	Supp Fig 1	unpaired t-test	Results, Para6	TRd=18, TRi=105	Modulation during reactivation vs downscaling from BMI1 to BMI2	Results, Para6	box plot with mean +/- SEM	Supp Fig1	0.4926	Supp Fig1	t(121)=-0.6883	Supp Fig1
+ -	Supp Fig 2	Regression	Results, Para6	TRd=18, TRi=105	MD reactivation of TRd and TRi cells versus their task modulation change from BMI1 to BMI2	Results, Para6	scatter plot	Supp Fig2	10e-5	Supp Fig2	R^2= 0.17	Supp Fig2
+ -	3c	one-way ANOVA	Results, Para8	TRd=18, TRi=105 in 3 conditions	Fano factor of TRd and TRi cells around task start and task end for successful and unsuccessful trials (in BMI fixed reward)	Results, Para8	box plot with mean +/- SEM	Fig 3c legend	2.6661e-33	Fig 3c legend	F(5,350)=41.2044	Fig 3c legend
+ -	3c	one-way ANOVA	Results, Para10	TRd=18, TRi=105 in fixed reward and TRd=6, TRi=41 in variable reward's task end	Fano factor of TRd and TRi cells around task end BMI fixed reward and BMI variable reward experiments	Results, Para10	box plot with mean +/- SEM	Fig 3c legend	4.4874e-33	Fig 3c legend	F(3,166)=83.8646	Fig 3c legend

+ -	4a	one-way ANOVA	Results, Para10	TRd-TRd pairs= 8; TRd-TRi pairs=10 in BMI fixed reward; TRd-TRd pairs= 2; TRd-TRi pairs=41 in BMI fixed reward;	Correlated firing around task start and end for TRd-TRd and TRd-TRi neurons in BMI fixed reward and BMI variable reward experiments (in task start and task end frames of reference)	Results, Para10	box plot with mean +/- SEM	Fig 4a legend	2.4089e-09	Fig 4a legend	F(7,304)=8.3592	Fig 4a legend
+ -	4b	Regression	Results, Para11	TRd-TRd pairs= 8; TRd-TRi pairs=105 with their respective MD reactivations in sleep	Correlated firing during reward (for BMI fixed reward experiments) vs MD reactivation in Sleep	Results, Para11	r squared	Fig 4b	P < 10e–21	Fig 4b	R^2= 0.54	Fig 4b
+ -	4c	Regression	Results, Para11	TRd-TRd pairs= 2; TRd-TRi pairs=41 with their respective MD reactivations in sleep	Correlated firing during reward (for BMI variable reward experiments) vs MD reactivation in Sleep	Results, Para 11	r squared	Fig 4c	P>0.05	Fig 4c	R^2= 0.07	Fig 4c
+ -	5c	one-way ANOVA	Results, Para12	OPTO_UP TRd= 17, OPTO_DOWN TRd= 14 OPTO_OFF TRd= 13	Modulation depth of TRd cells in OPTO_UP, OPTO_DOWN and OPTO_OFF experiments from pre sleep to post sleep	Fig 5c legend	box plot with mean +/- SEM	Fig 5c legend	3.755e-28	Fig 5c legend	F(2,41)=425.745	Fig 5c legend
+ -	5f	one-way ANOVA	Results, Para12	OPTO_UP=11 sessions; OPTO_DOWN=8 sessions; OPTO_OFF= 8 sessions	PSD changes in OPTO_UP, OPTO_DOWN and OPTO_OFF experiments from pre sleep to post sleep	Fig 5f legend	box plot with mean +/- SEM	Fig 5c legend	0.8749	Fig 5c legend	F(2,27)=0.1344	Fig 5c legend
+ -	NA	Spearman Correlation	Results, Para2	10 pairs	Time spent in sleep vs extent of TRi rescaling	Results, Para2	correlation	Results, Para2	0.0101	Results, Para2	r=0.7148	Results, Para2
+ -	NA	Wilcoxon signed rank test	Results, Para2	18 pairs	TRd modulation in BMI1 vs BMI2	Results, Para2	mean +/- SEM	Results, Para2	0.0352	Results, Para2	Z=-1.8092	Results, Para2
+ -	NA	paired t-test	Results, Para2	105 pairs	TRi modulation in BMI1 vs BMI2	Results, Para2	mean +/- SEM	Results, Para2	3.43e-27	Results, Para2	t(104)=14.5805	Results, Para2
+ -	NA	paired t-test	Results, Para2	10 pairs	Pre and Post Sleep durations	Results, Para2	mean +/- SEM (for Sleep post)	Results, Para2	0.9560	Results, Para2	t(9)=0.0567	Results, Para2
+ -	NA	paired t-test	Results, Para3	18 pairs	Sleep epochs firing rates (Watson style), TRd	Results, Para3	mean +/- SEM	Results, Para3	0.1184	Results, Para3	t(17)=-1.6446	Results, Para3

+ -	NA	paired t-test	Results, Para3	105 pairs	Sleep epochs firing rates (Watson style), TRi	Results, Para3	mean +/- SEM	Results, Para3	0.9605	Results, Para3	t(104)=-0.0497	Results, Para3
+ -	NA	one-way ANOVA	Results, Para8	TRd=18, TRi=105 in 2 conditions	Fano factor of TRd and TRi cells around task start and task end in BMI fixed reward at equal firing rate activity	Results, Para8	mean +/- SEM	Results, Para8	1.9794e-10	Results, Para8	F(3,242)=17.7181	Results, Para8
+ -	NA	paired t-test	Results, Para9	4 BMI variable reward sessions	BMI variable reward task performance change from BMI1Early to BMI1Late	Results, Para9	mean +/- SEM (for change)	Results, Para9	0.0105	Results, Para9	t(3)=4.464	Results, Para9
+ -	NA	paired t-test	Results, Para9	TRd=6, in BMI variable reward experiments	BMI variable reward neurons MD change from BMI1 to BMI2	Results, Para9	mean +/- SEM (for change)	Results, Para9	0.1086	Results, Para9	t(5)=-1.9508	Results, Para9
+ -	NA	paired t-test	Results, Para9	TRi=41 in BMI variable reward experiments	BMI variable reward neurons MD change from BMI1 to BMI2	Results, Para9	mean +/- SEM (for change)	Results, Para9	0.1503	Results, Para9	t(40)=-1.4666	Results, Para9
+ -	NA	Spearman correlation	Results, Para11	TRd-TRd pairs= 8; TRd-TRi pairs=105 with their respective MD reactivations in sleep	Correlated firing during task start (for BMI fixed reward experiments) vs MD reactivation in Sleep	Results, Para11	correlation value	Results, Para11	P = 0.19	Results, Para11	r = 0.12	Results, Para11
+ -	Supp Fig 3a	unpaired t-test	Results, Para12	OPTO_UP=11 sessions; OPTO_DOWN=8 sessions	100 ms stimulation pulse incidence during OPTO_UP and OPTO_DOWN experiments	Results, Para12	box plot with mean +/- SEM	Supp Fig 3a	0.3338	Supp Fig 3a	t(17)=0.9947	Supp Fig 3a
+ -	Supp Fig 3a	unpaired t-test	Results, Para12	OPTO_UP=11 sessions; OPTO_DOWN=8 sessions	100 ms stimulation duration proportion to total NREM sleep during OPTO_UP and OPTO_DOWN experiments	Results, Para12	box plot with mean +/- SEM	Supp Fig 3b	0.0538	Supp Fig 3b	t(17)=2.0721	Supp Fig 3b
+ -	Supp Fig 4	one-way ANOVA	Results, Para12	OPTO_UP=11 sessions; OPTO_DOWN=8 sessions; OPTO_OFF= 8 sessions	Pre sleep and post sleep durations in OPTO_UP, OPTO_DOWN, and OPTO_OFF experiments	Results, Para12	box plot with mean +/- SEM	Supp Fig 4	0.4740	Supp Fig 4	F(5,48)=0.9235	Supp Fig 4
+ -	6b	paired t-test	Results, Para13	OPTO_UP=11 sessions	Performance changes in OPTO_UP experiments from BMI1 late to BMI2 early (both tail)	Fig 6b legend	All individual session changes are shown	Fig 6b legend	3.8955e-04	Fig 6b legend	t(10)= -5.22	Fig 6b legend

+ -	6b	paired t-test	Results, Para13	OPTO_DOWN=8 sessions	Performance changes in OPTO_DOWN experiments from BMI1 late to BMI2 early	Fig 6b legend	All individual session changes are shown	Fig 6b legend	6.822e-04	Fig 6b legend	t(7)=5.122	Fig 6b legend
+ -	6b	paired t-test	Results, Para13	OPTO_OFF=8 sessions	Performance changes in OPTO_OFF experiments from BMI1 late to BMI2 early	Fig 6b legend	All individual session changes are shown	Fig 6b legend	5.640e-05	Fig 6b legend	t(7)=7.73	Fig 6b legend
+ -	NA	one-way ANOVA	Results, Para13	TRd=17, TRi=95 in 2 frames	Fano factor of TRd and TRi neurons in OPTO_UP experiments in BMI2 in task start and task-end frames of references	Results, Para13	mean +/- SEM	Results, Para13	0.7229	Results, Para13	F(3,220)=0.4423	Results, Para13
+ -	7a	unpaired t-test	Results, Para14	TRd=17, TRi=95	MD change of TRd and TRi neurons in OPTO_UP experiments from BMI1 to BMI2	Fig 7a legend	box plot with mean +/- SEM	Fig 7a legend	0.64059	Fig 7a legend	t(110)= -0.46816	Fig 7a legend
+ -	7a	unpaired t-test	Results, Para14	TRd=14, TRi=94	MD change of TRd and TRi neurons in OPTO_DOWN experiments from BMI1 to BMI2	Fig 7a legend	box plot with mean +/- SEM	Fig 7a legend	3.883e-04	Fig 7a legend	t(106)= 3.6649	Fig 7a legend
+ -	7a	unpaired t-test	Results, Para14	TRd=13, TRi=62	MD change of TRd and TRi neurons in OPTO_OFF experiments from BMI1 to BMI2	Fig 7a legend	box plot with mean +/- SEM	Fig 7a legend	5.0074e-07	Fig 7a legend	t(73)= 5.5155	Fig 7a legend
+ -	NA	paired t-test	Discussion, Para 5	TRd=17	MD change of TRd neurons from BMI1 to BMI2 in OPTO_UP experiments	Discussion, Para 5	mean +/- SEM	Discussion, Para 5	0.02024	Discussion, Para 5	t(16)= -2.229	Discussion, Para 5
+ -	NA	paired t-test	Discussion, Para 5	TRi=95	MD change of TRd neurons from BMI1 to BMI2 in OPTO_UP experiments	Discussion, Para 5	mean +/- SEM	Discussion, Para 5	6.691e-10	Discussion, Para 5	t(94)= -6.727	Discussion, Para 5
+ -	7c	one-way ANOVA	Results, Para14	OPTO_UP=17 neurons; OPTO_DOWN=15 neurons; OPTO_OFF= 13 neurons	SFC change of TRd neurons from pre sleep and post sleep in OPTO_UP, OPTO_DOWN, and OPTO_OFF experiments	Results, Para14	box plot with mean +/- SEM	Fig 7c legend	4.79701e-11	Fig 7c legend	F(2,41)=44.831	Fig 7c legend
+ -	7d	regression	Results, Para14	OPTO_UP=11 sessions; OPTO_DOWN=8 sessions; OPTO_OFF= 8 sessions	Averaged TRd SFC change from Sleep pre to Sleep post versus averaged TRi rescaling from BMI1 to BMI2 in OPTO_UP, OPTO_DOWN, and OPTO_OFF experiments	Results, Para14	r-squared	Fig 7d legend	10e-6	Fig 7d legend	R^2=0.66	Fig 7d legend
+ -	NA	paired t-test	Results, Para 7	18 pairs	TRd modulation around task start vs task end	Results, Para 7	mean +/- SEM	Results, Para 7	3.0599e-06	Results, Para 7	t(17)= -6.8061	Results, Para 7

+ -	NA	paired t-test	Results, Para 7	105 pairs	TRd modulation around task start vs task end	Results, Para 7	mean +/- SEM	Results, Para 7	0.0531	Results, Para 7	t(104)= 1.9565	Results, Para 7

Representative figures

1. Are any representative images shown (including Western blots and immunohistochemistry/staining) in the paper?

   If so, what figure(s)?

Yes, following figures show representative performance improvements after sleep, Modulation depth changes after sleep (for direct, TR_d and indirect, TR_i neurons), spike spike coherence changes in sleep sessions before and after BMI training, modulation around reactivation in pre and post sleep, modulation around task start and task end, fano factor in same frames for BMI fixed and variable reward optogenetic inhibition around slow-wave activity in UP, DOWN and OFF experiments, and behavioral learning curves in them, SFC changes in them, 100 ms stimulation pulses incidence and proportion in them, durations of sleep in different kinds of experiments: Fig. 1c,e; Fig 2a,c-e; Fig. 3a,c; Fig. 4a; Fig 5c,f; Fig 6b; Fig 7a,d; Supp Fig 1, Supp Fig 3a,b; Supp Fig 4.

2. For each representative image, is there a clear statement of how many times this experiment was successfully repeated and a discussion of any limitations in repeatability?

   If so, where is this reported (section, paragraph #)?

Yes:
Fig. 1: Results para 1 and 2 ; and methods para 1,3,4 8
Fig. 2: Results para 3 and 6 ; and methods para 1,3,4 8
Fig. 3: Results para 8 and 10 ; and methods para 1,3,4 8
Fig. 4: Results para 10 and 11 ; and methods para 1,3,4 8
Fig. 5: Results para 12 ; and methods para 1,7
Fig. 6: Results para 13 ; and methods para 1,7
Fig. 7: Results para 14 ; and methods para 1,7

Supp Fig 1: Results para 6; and methods para 1,3,4 8
Supp Fig 3: Results para 12 ; and methods para 1,7
Supp Fig 4: Results para 12 ; and methods para 1,7

Statistics and general methods

1. Is there a justification of the sample size?

   If so, how was it justified?

   Where (section, paragraph #)?

   Even if no sample size calculation was performed, authors should report why the sample size is adequate to measure their effect size.

Our sample size is similar to what is usually used to establish task-related consolidation during sleep, or task-related neural modulation in other studies (for example, n ranging from 5 to 12 in in our references). This is stated in online methods, paragraph 1. Number of neurons analyzed in each group are summarized in online methods, paragraph 18.

2. Are statistical tests justified as appropriate for every figure?

   Where (section, paragraph #)?

Yes, in the result sections and methods section appropriate tests are listed. Online methods section, paragraph 18 summarizes these.

   a. If there is a section summarizing the statistical methods in the methods, is the statistical test for each experiment clearly defined?

Yes, online methods section, paragraph 18 summarizes these.

   b. Do the data meet the assumptions of the specific statistical test you chose (e.g. normality for a parametric test)?

      Where is this described (section, paragraph #)?

Yes, we substituted for non-parametric test wherever sample distribution failed the test of normality and this was detailed in methods (paragraph on statistical tests), paragraph 18.

c. Is there any estimate of variance within each group of data?

Is the variance similar between groups that are being statistically compared?

Where is this described (section, paragraph #)?

For one-way ANOVA, test for homogeneity of variances was done. It's is described in methods, paragraph 18.

d. Are tests specified as one- or two-sided?

Yes. In main text as well as methods.

e. Are there adjustments for multiple comparisons?

Not required as ANOVA was significant. Multiple t-test was used for post-hoc tests.

3. To promote transparency, *Nature Neuroscience* has stopped allowing bar graphs to report statistics in the papers it publishes. If you have bar graphs in your paper, please make sure to switch them to dot-plots (with central and dispersion statistics displayed) or to box-and-whisker plots to show data distributions.

Yes, dot plots with dispersion statistics are included.

4. Are criteria for excluding data points reported?

Was this criterion established prior to data collection?

Where is this described (section, paragraph #)?

Not applicable. Except Units with high SNR were used for subsequent analysis (see Methods paragraph 3).

5. Define the method of randomization used to assign subjects (or samples) to the experimental groups and to collect and process data.

If no randomization was used, state so.

Where does this appear (section, paragraph #)?

For the optogenetic experiments, sometimes the non-stimulation experiments were done before stimulation or sometimes after optogenetic stimulation experiments. Hence this control was randomized, otherwise there was no blinding, as stated in online methods, paragraph 1.

6. Is a statement of the extent to which investigator knew the group allocation during the experiment and in assessing outcome included?

If no blinding was done, state so.

Where (section, paragraph #)?

No blinding was done, as stated in online methods, paragraph 1.

7. For experiments in live vertebrates, is a statement of compliance with ethical guidelines/regulations included?

Where (section, paragraph #)?

Yes, Methods: paragraph 01

8. Is the species of the animals used reported?

Where (section, paragraph #)?

Yes, Methods: paragraph 01

9. Is the strain of the animals (including background strains of KO/ transgenic animals used) reported?

Where (section, paragraph #)?

Yes, Methods: paragraph 01

10. Is the sex of the animals/subjects used reported?

Where (section, paragraph #)?

Yes, Methods: paragraph 01

11. Is the age of the animals/subjects reported?

    Where (section, paragraph #)?

It's not reported. But all animals were adult male rats. They were procured at body weight ~250 gm (approximately 8 weeks age). Experiments were initiated within 5 days of delivery.

12. For animals housed in a vivarium, is the light/dark cycle reported?

    Where (section, paragraph #)?

Yes, Methods paragraph 01

13. For animals housed in a vivarium, is the housing group (i.e. number of animals per cage) reported?

    Where (section, paragraph #)?

Not reported but prior to surgery there were 2 rats/ cage. After surgery we put 1 rat/ cage due to water feeding restriction schedule.

14. For behavioral experiments, is the time of day reported (e.g. light or dark cycle)?

    Where (section, paragraph #)?

Yes, Methods paragraph 01

15. Is the previous history of the animals/subjects (e.g. prior drug administration, surgery, behavioral testing) reported?

    Where (section, paragraph #)?

Yes, Methods paragraph 01 and 02

    a. If multiple behavioral tests were conducted in the same group of animals, is this reported?

       Where (section, paragraph #)?

Yes, Methods paragraph Animals and Behavior

16. If any animals/subjects were excluded from analysis, is this reported?

    Where (section, paragraph #)?

Not applicable

    a. How were the criteria for exclusion defined?

       Where is this described (section, paragraph #)?

NA

    b. Specify reasons for any discrepancy between the number of animals at the beginning and end of the study.

       Where is this described (section, paragraph #)?

NA

Reagents

1. Have antibodies been validated for use in the system under study (assay and species)?

NA

    a. Is antibody catalog number given?

       Where does this appear (section, paragraph #)?

NA

b. Where were the validation data reported (citation, supplementary information, Antibodypedia)?

Where does this appear (section, paragraph #)?

NA

2. Cell line identity

a. Are any cell lines used in this paper listed in the database of commonly misidentified cell lines maintained by ICLAC and NCBI Biosample?

Where (section, paragraph #)?

NA

b. If yes, include in the Methods section a scientific justification of their use--indicate here in which section and paragraph the justification can be found.

NA

c. For each cell line, include in the Methods section a statement that specifies:

- the source of the cell lines
- have the cell lines been authenticated? If so, by which method?
- have the cell lines been tested for mycoplasma contamination?

Where (section, paragraph #)?

NA

Data availability

Provide a Data availability statement in the Methods section under "Data availability", which should include, where applicable:

- Accession codes for deposited data
- Other unique identifiers (such as DOIs and hyperlinks for any other datasets)
- At a minimum, a statement confirming that all relevant data are available from the authors
- Formal citations of datasets that are assigned DOIs
- A statement regarding data available in the manuscript as source data
- A statement regarding data available with restrictions

See our data availability and data citations policy page for more information.

Data deposition in a public repository is mandatory for:

a. Protein, DNA and RNA sequences
b. Macromolecular structures
c. Crystallographic data for small molecules
d. Microarray data

Deposition is strongly recommended for many other datasets for which structured public repositories exist; more details on our data policy are available here. We encourage the provision of other source data in supplementary information or in unstructured repositories such as Figshare and Dryad.

We encourage publication of Data Descriptors (see Scientific Data) to maximize data reuse.

Where is the Data Availability statement provided (section, paragraph #)?

Data availability
The data that support the findings of this study are available from the corresponding author upon request.

Computer code/software

Any custom algorithm/software that is central to the methods must be supplied by the authors in a usable and readable form for readers at the time of publication. However, referees may ask for this information at any time during the review process.

1. Identify all custom software or scripts that were required to conduct the study and where in the procedures each was used.

We have used open-source (for example Chronux, ensemble reactivation analysis), as well as in built and custom script in Matlab (for example statistical tests;,finding sleep epochs, performance gains, modulation depth, etc.)

2. If computer code was used to generate results that are central to the paper's conclusions, include a statement in the Methods section under "**Code availability**" to indicate whether and how the code can be accessed. Include version information as necessary and any restrictions on availability.

A statement of code availability is included in Methods (Data and code availability sub-section) and specific code is available. We also make clear where publicly available code (for example Chronux toolkit) used in this study can be found.

Human subjects

1. Which IRB approved the protocol?

   Where is this stated (section, paragraph #)?

NA for all topics in this section

2. Is demographic information on all subjects provided?

   Where (section, paragraph #)?

3. Is the number of human subjects, their age and sex clearly defined?

   Where (section, paragraph #)?

4. Are the inclusion and exclusion criteria (if any) clearly specified?

   Where (section, paragraph #)?

5. How well were the groups matched?

   Where is this information described (section, paragraph #)?

6. Is a statement included confirming that informed consent was obtained from all subjects?

   Where (section, paragraph #)?

7. For publication of patient photos, is a statement included confirming that consent to publish was obtained?

   Where (section, paragraph #)?

fMRI studies

For papers reporting functional imaging (fMRI) results please ensure that these minimal reporting guidelines are met and that all this information is clearly provided in the methods:

1. Were any subjects scanned but then rejected for the analysis after the data was collected?

NA for all topics in this section

   a. If yes, is the number rejected and reasons for rejection described?

      Where (section, paragraph #)?

2. Is the number of blocks, trials or experimental units per session and/or subjects specified?

   Where (section, paragraph #)?

3. Is the length of each trial and interval between trials specified?

4. Is a blocked, event-related, or mixed design being used? If applicable, please specify the block length or how the event-related or mixed design was optimized.

5. Is the task design clearly described?

   Where (section, paragraph #)?

6. How was behavioral performance measured?

7. Is an ANOVA or factorial design being used?

8. For data acquisition, is a whole brain scan used?

   If not, state area of acquisition.

   a. How was this region determined?

9. Is the field strength (in Tesla) of the MRI system stated?

   a. Is the pulse sequence type (gradient/spin echo, EPI/spiral) stated?

   b. Are the field-of-view, matrix size, slice thickness, and TE/TR/flip angle clearly stated?

10. Are the software and specific parameters (model/functions, smoothing kernel size if applicable, etc.) used for data processing and pre-processing clearly stated?

11. Is the coordinate space for the anatomical/functional imaging data clearly defined as subject/native space or standardized stereotaxic space, e.g., original Talairach, MNI305, ICBM152, etc? Where (section, paragraph #)?

12. If there was data normalization/standardization to a specific space template, are the type of transformation (linear vs. nonlinear) used and image types being transformed clearly described? Where (section, paragraph #)?

13. How were anatomical locations determined, e.g., via an automated labeling algorithm (AAL), standardized coordinate database (Talairach daemon), probabilistic atlases, etc.?

14. Were any additional regressors (behavioral covariates, motion etc) used?

15. Is the contrast construction clearly defined?

16. Is a mixed/random effects or fixed inference used?

   a. If fixed effects inference used, is this justified?

17. Were repeated measures used (multiple measurements per subject)?

a. If so, are the method to account for within subject correlation and the assumptions made about variance clearly stated?

18. If the threshold used for inference and visualization in figures varies, is this clearly stated?

19. Are statistical inferences corrected for multiple comparisons?

a. If not, is this labeled as uncorrected?

20. Are the results based on an ROI (region of interest) analysis?

a. If so, is the rationale clearly described?

b. How were the ROI's defined (functional vs anatomical localization)?

21. Is there correction for multiple comparisons within each voxel?

22. For cluster-wise significance, is the cluster-defining threshold and the corrected significance level defined?

Additional comments

Additional Comments